US 20240271253A1

(19) **United States**

(12) **Patent Application Publication** (10) **Pub. No.: US 2024/0271253 A1**

MANUEL et al. (43) **Pub. Date: Aug. 15, 2024**

(54) **MAGNESIUM-LITHIUM ALLOYS COMPOSED OF GALLIUM OR INDIUM**

(71) Applicant: **University of Florida Research Foundation, Inc.**, Gainesville, FL (US)

(72) Inventors: **Michele V. MANUEL**, Gainesville, FL (US); **David Wesley CHRISTIANSON**, Gainesville, FL (US)

(21) Appl. No.: **18/567,951**

(22) PCT Filed: **Jun. 6, 2022**

(86) PCT No.: **PCT/US2022/032291**

§ 371 (c)(1),
(2) Date: **Dec. 7, 2023**

Related U.S. Application Data

(60) Provisional application No. 63/197,623, filed on Jun. 7, 2021.

Publication Classification

(51) **Int. Cl.**

C22C 23/00	(2006.01)
C22C 1/02	(2006.01)
C22F 1/06	(2006.01)

(52) **U.S. Cl.**

CPC ***C22C 23/00*** (2013.01); ***C22C 1/02*** (2013.01); ***C22F 1/06*** (2013.01)

(57) **ABSTRACT**

Described herein are Mg—Li alloys composed of gallium or indium. The amount of gallium or indium incorporated into the alloys enhances the physical properties of the alloys. For example, the addition of gallium or indium strengthens the alloys and makes them harder and tougher. In one aspect, the Mg—Li alloys described herein include gallium in the amount of from about 0.1 atomic percent to about 2 atomic percent or from about 0.5 weight percent to about 10 weight percent. In another aspect, the Mg—Li alloys described herein include indium in the amount of from about 0.1 atomic percent to about 2 atomic percent or from about 2 weight percent to about 15 weight percent. The alloys described herein have numerous applications where it is desirable to produce articles that are light-weight yet very strong and hard.

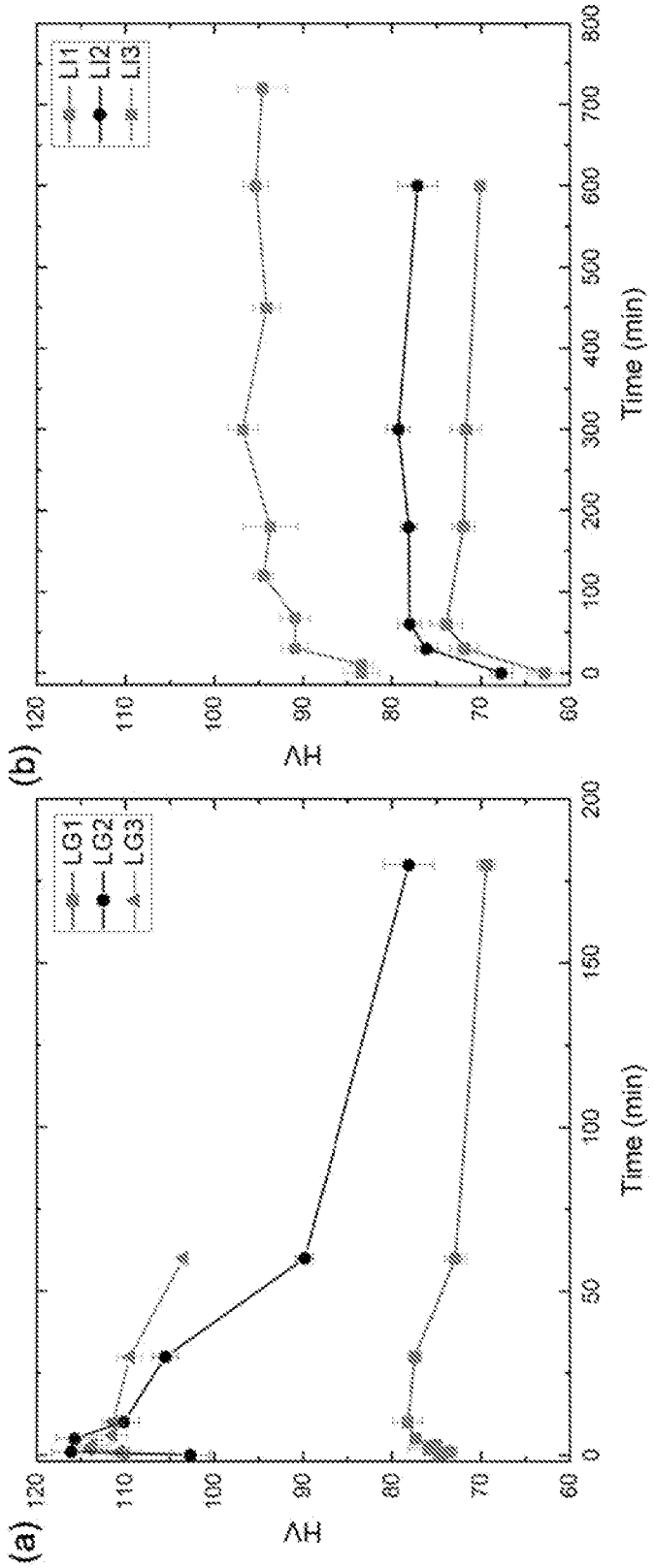

FIGS. 1A-1B

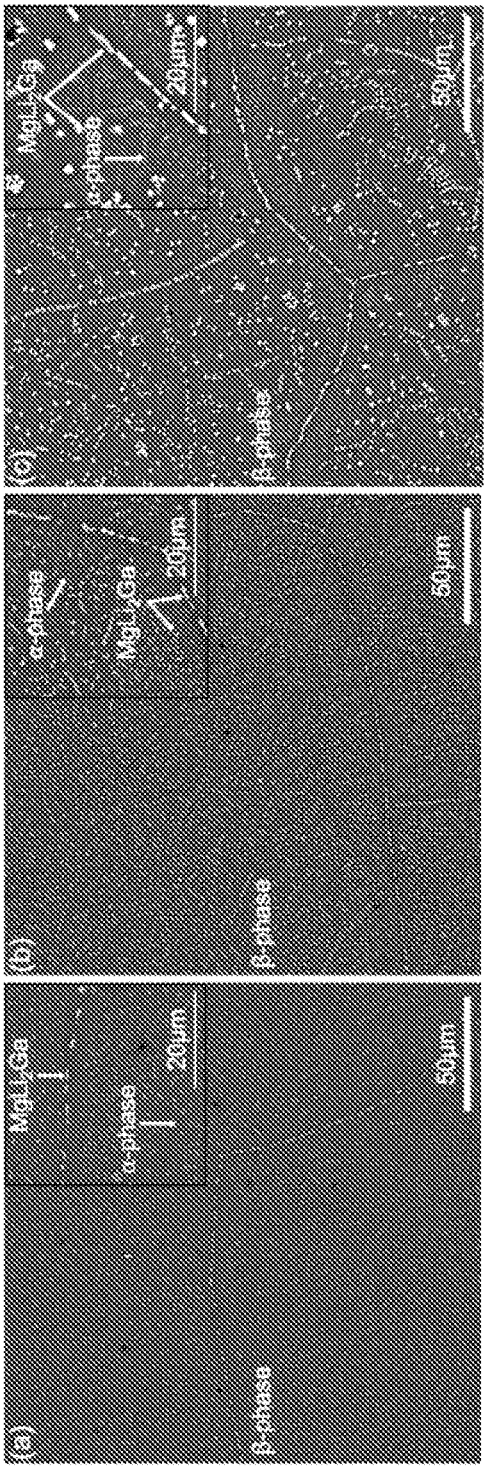
(a)
Mg$_2$Ga$_5$O$_8$
α-phase
20μm
β-phase
50μm
(b)
α-phase
Mg$_2$Ga$_5$O$_8$
20μm
β-phase
50μm
(c)
Mg$_2$Ga$_5$O$_8$
α-phase
20μm
β-phase
50μm

FIGS. 2A-2C

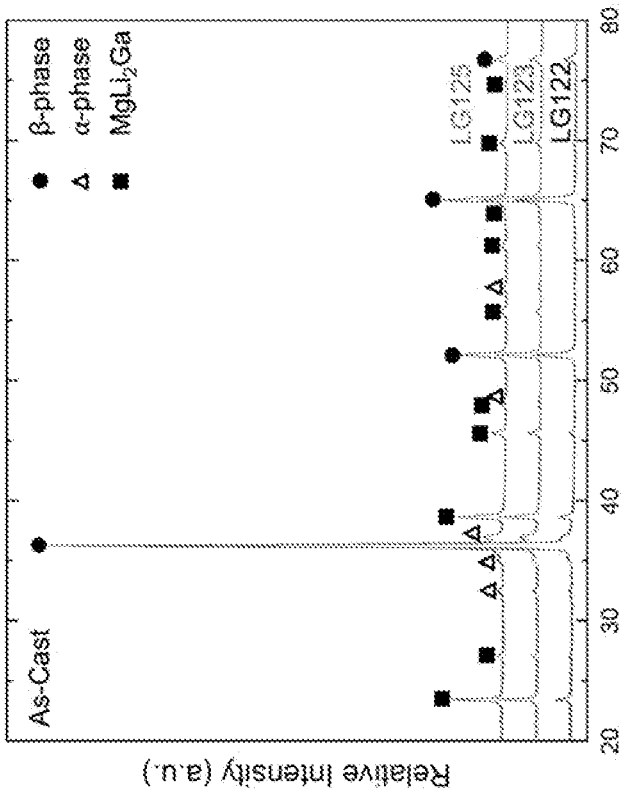
As-Cast
β-phase
α-phase
MgLi2Ga
LG125
LG123
LG122
Relative Intensity (a.u.)
2θ (°)
20
30
40
50
60
70
80

FIG. 3

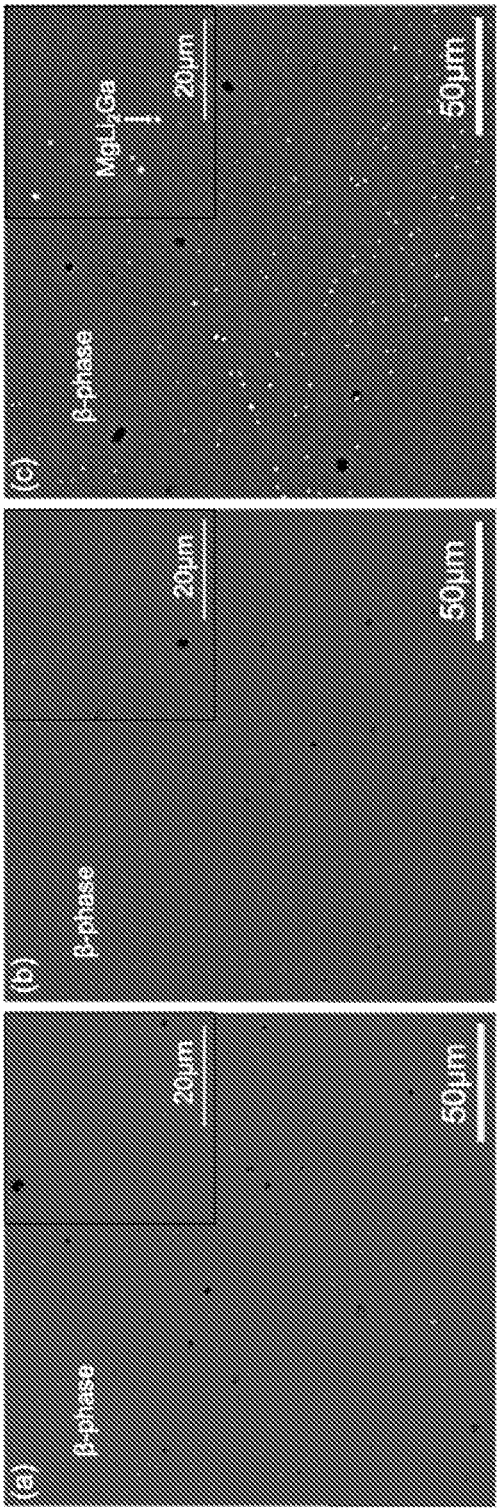
(a)
β-phase
20μm
50μm
(b)
β-phase
20μm
50μm
(c)
β-phase
Mg$_{17}$Ga$_{12}$
20μm
50μm

FIGS. 4A-4C

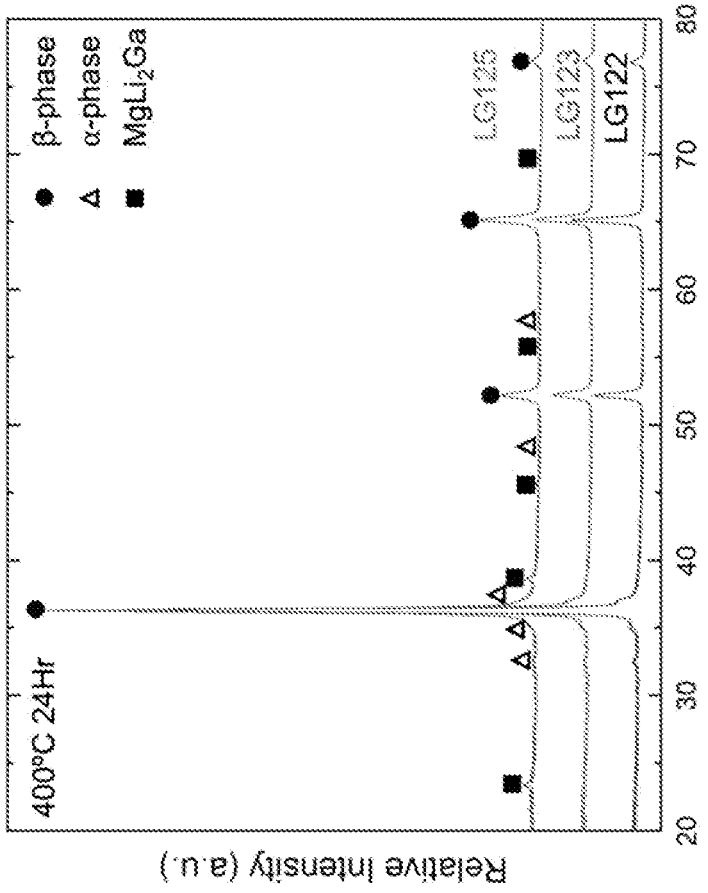
400°C 24Hr
β-phase
α-phase
MgLi2Ga
LG125
LG123
LG122
Relative Intensity (a.u.)
2θ (°)
20
30
40
50
60
70
80

FIG. 5

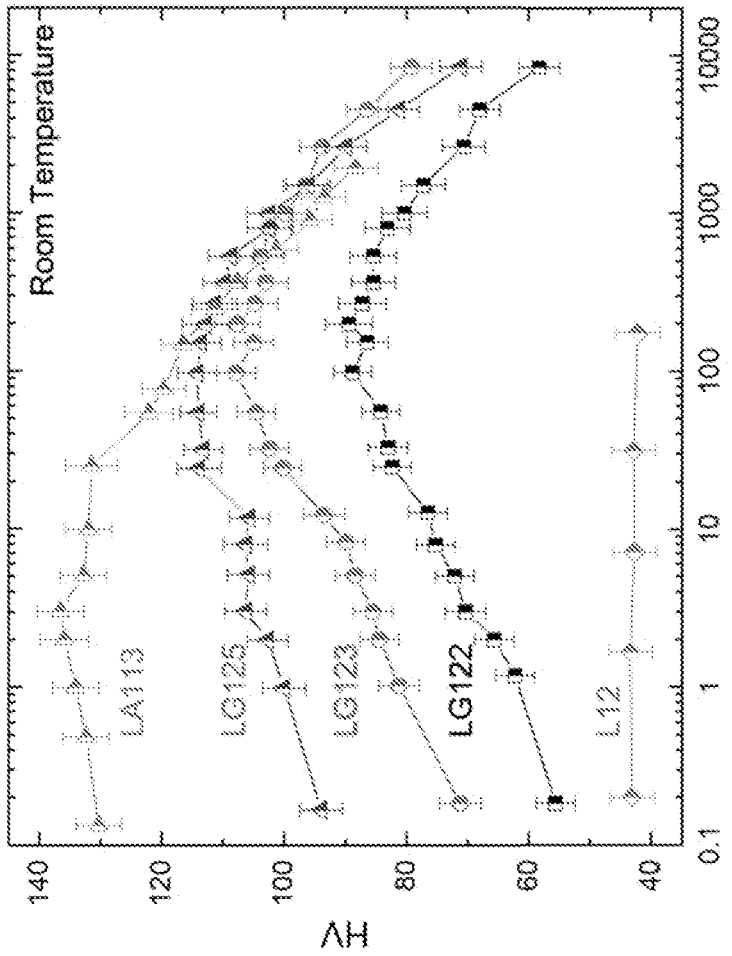
Room Temperature
LA113
LG125
LG123
LG122
L12
HV
Time (Hr)
140
120
100
80
60
40
0.1
1
10
100
1000
10000

FIG. 6

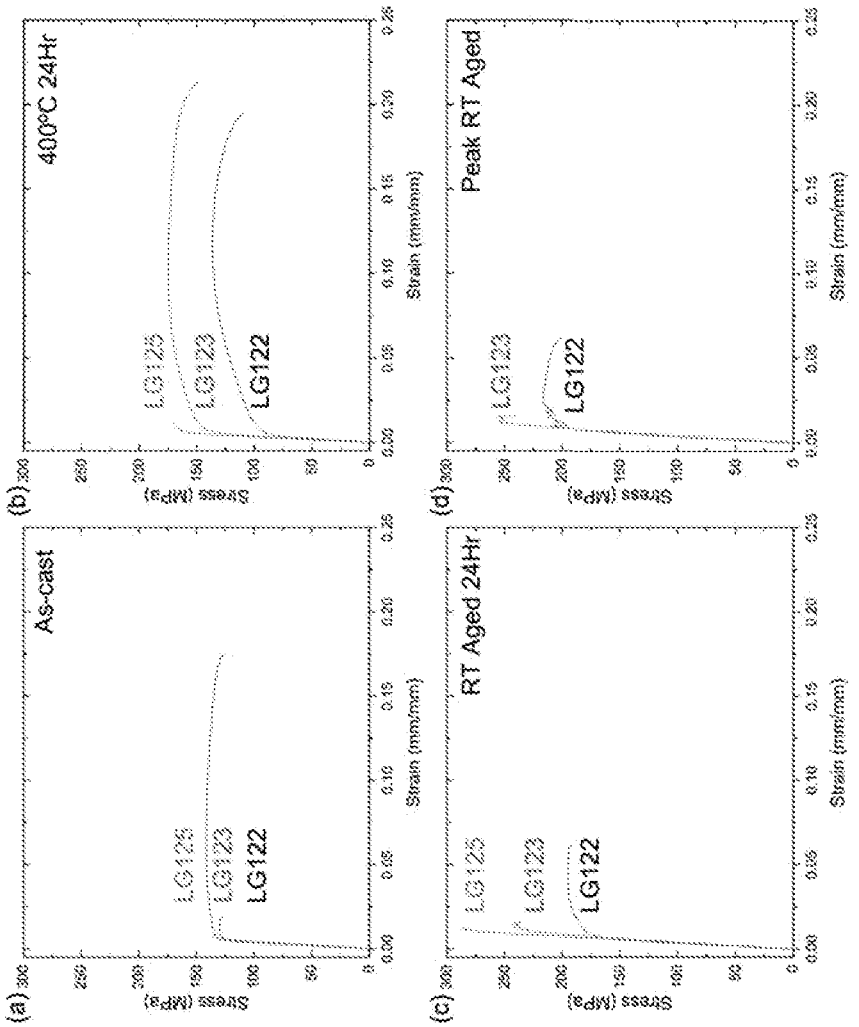
(a)
As-cast
LG125
LG123
LG122
(b)
400°C 24Hr
LG125
LG123
LG122
(c)
RT Aged 24Hr
LG125
LG123
LG122
(d)
Peak RT Aged
LG123
LG122
Stress (MPa)
Strain (mm/mm)

FIGS. 7A-7D

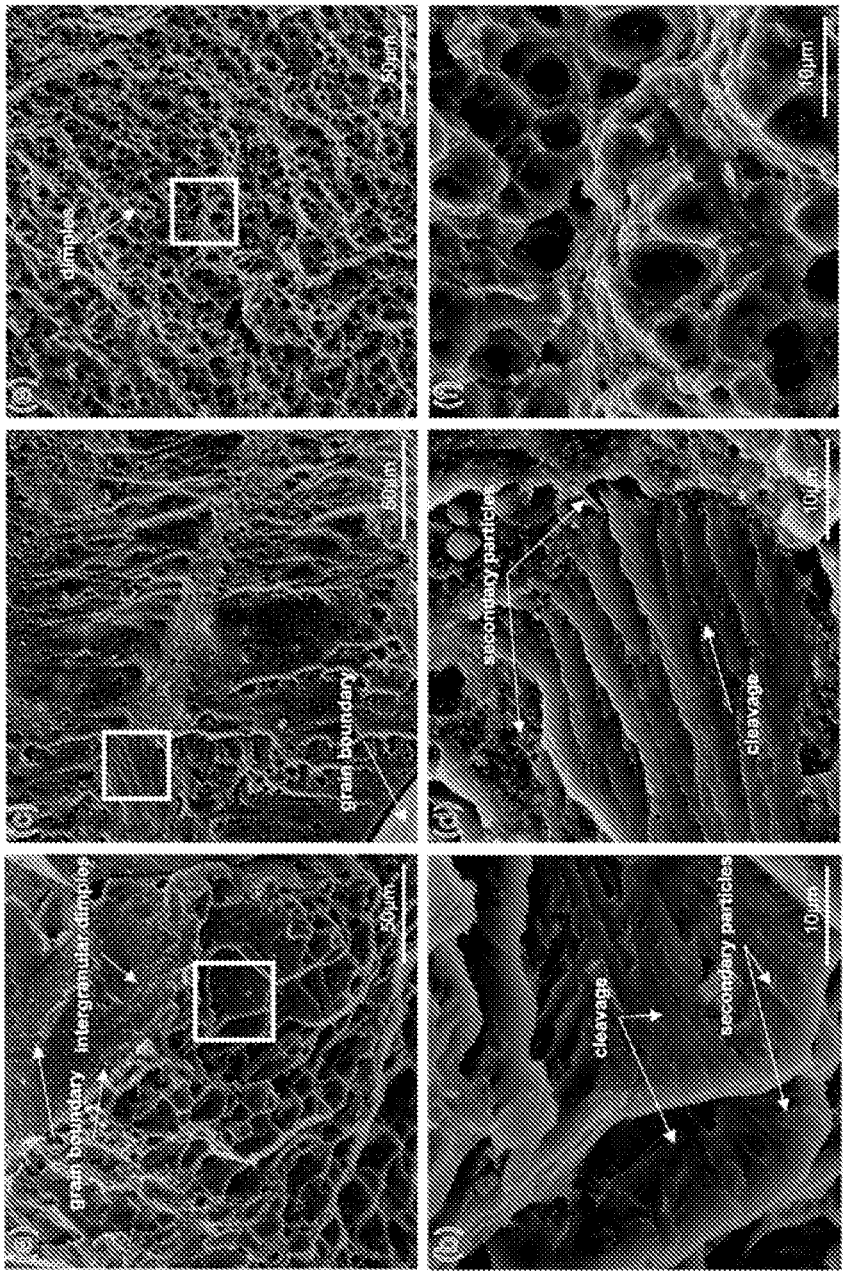
(a)
grain boundary
intergranular dimple
50μm
(b)
grain boundary
50μm
(c)
dimple
50μm
(d)
cleavage
secondary particle
10μm
(e)
secondary particle
cleavage
10μm
(f)
10μm

FIGS. 8A-8F

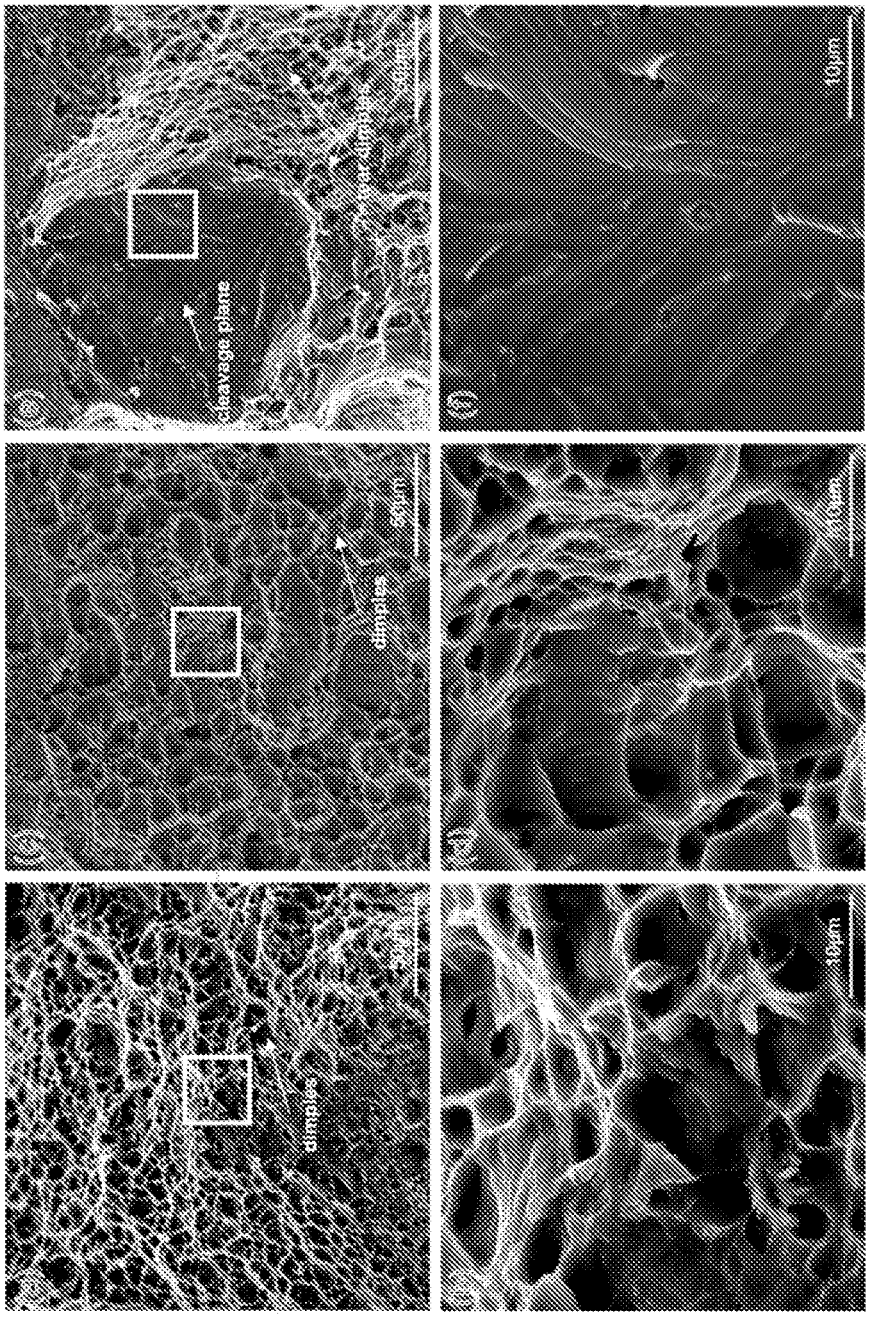

FIGS. 9A-9F

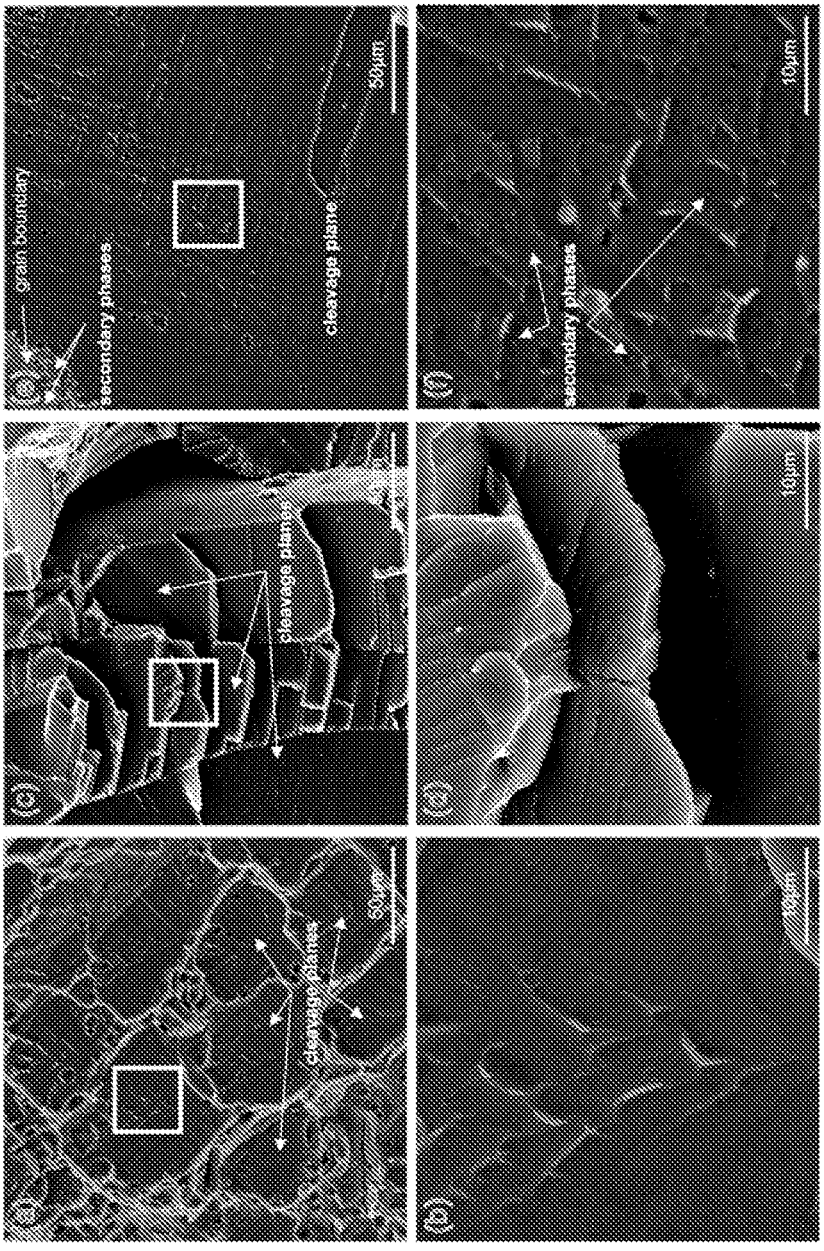
(a)
Grain boundary
Secondary cracks
50μm
(b)
cleavage plane
50μm
(c)
cleavage plane
50μm
(d)
Secondary cracks
10μm
(e)
Secondary cracks
50μm
(f)
10μm
(g)
10μm

FIGS. 10A-10F

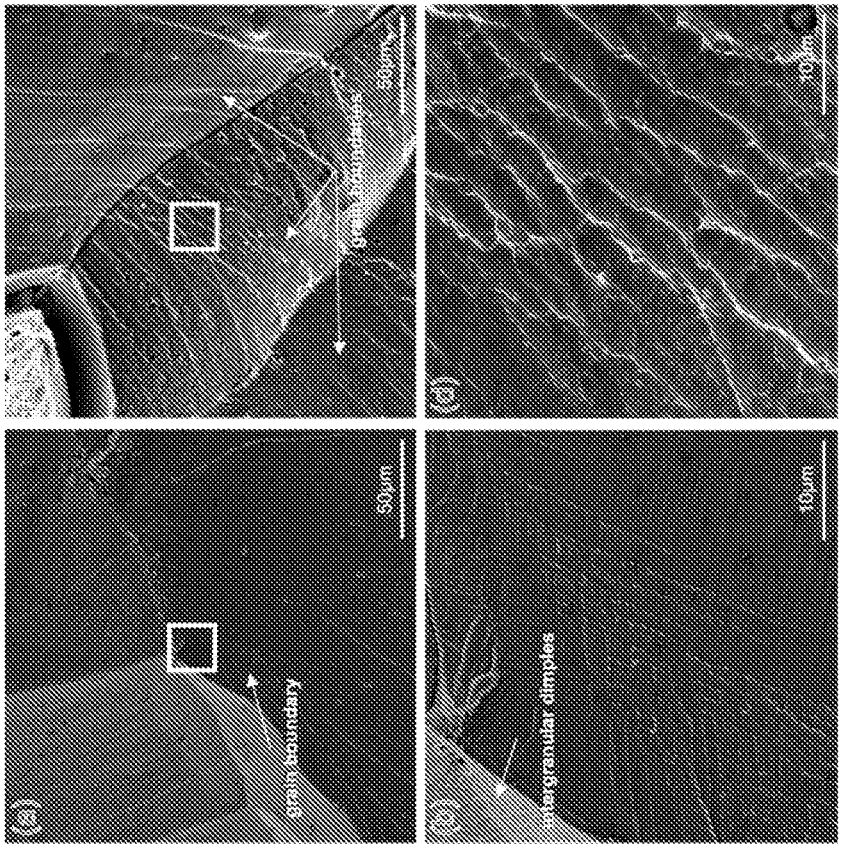
(a)
grain boundary
50μm
(b)
Crack direction
50μm
(c)
intergranular dimples
10μm
(d)
10μm

FIGS. 11A-11D

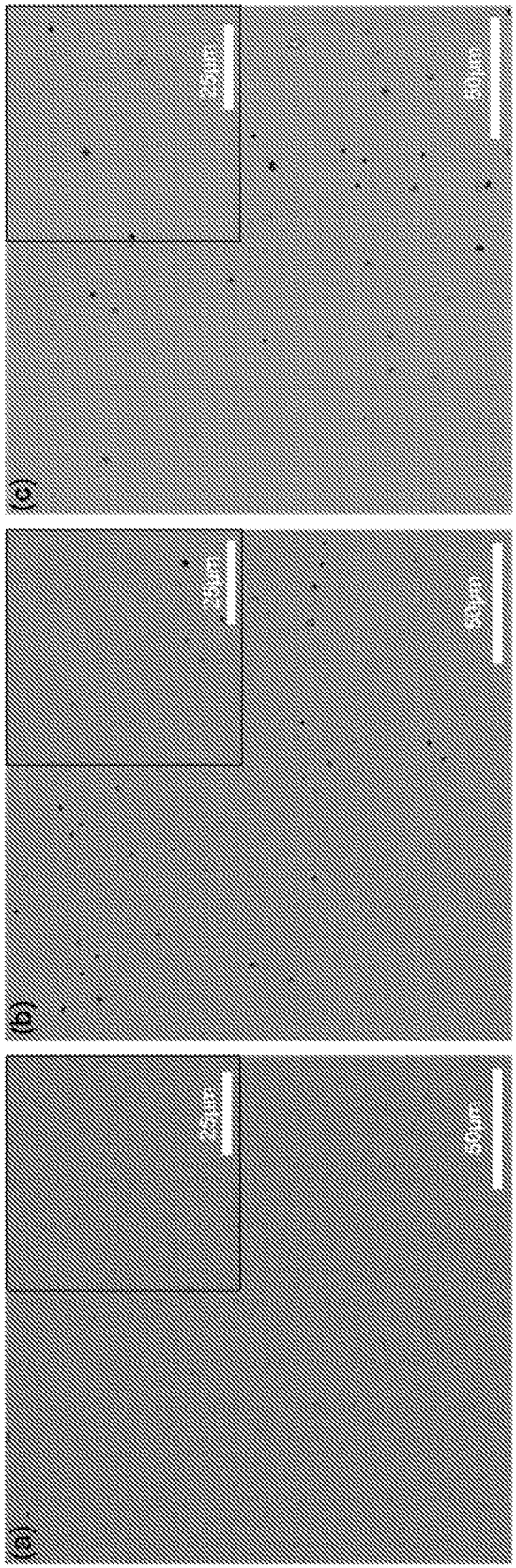

FIGS. 12A-12C

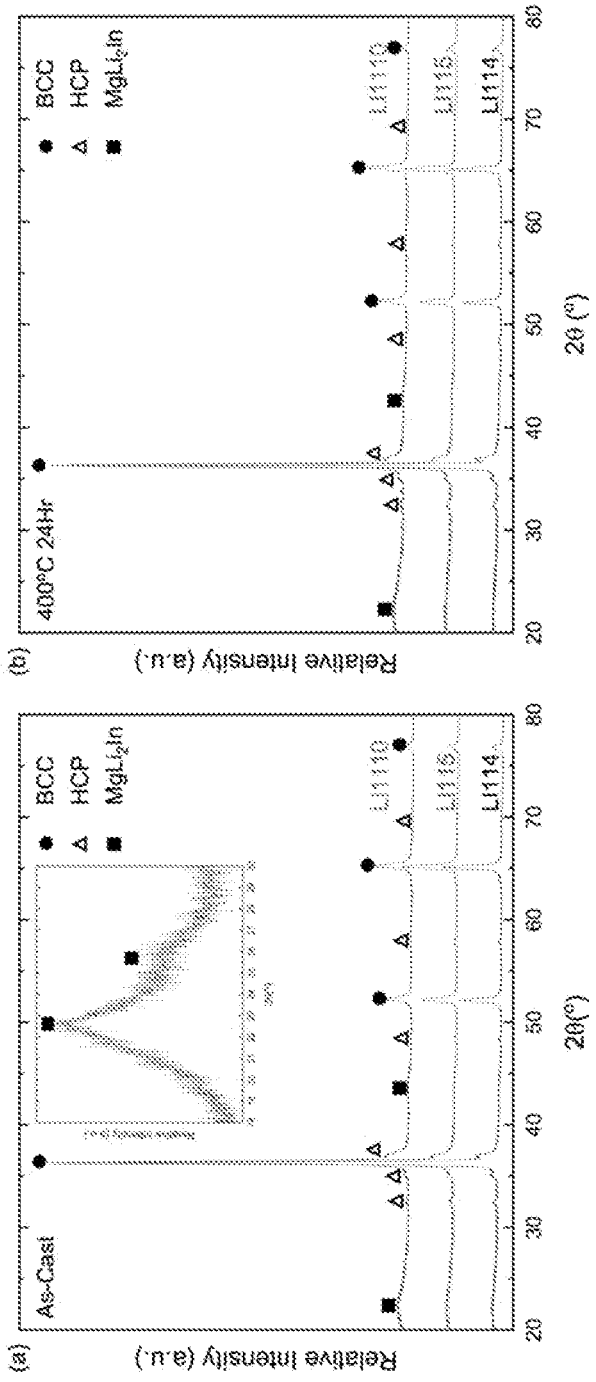
(a)
As-Cast
BCC
HCP
$MgLi_2In$
L11110
L1116
L1114
Relative Intensity (a.u.)
2θ(°)
(b)
400°C 24Hr
BCC
HCP
$MgLi_2In$
L11110
L1116
L1114
Relative Intensity (a.u.)
2θ (°)

FIGS. 13A-13B

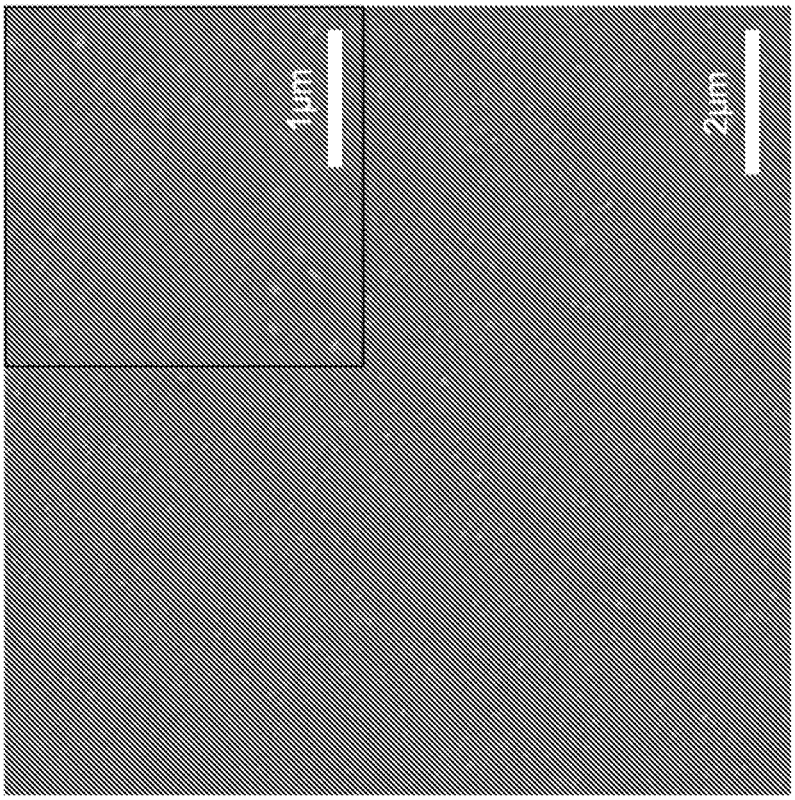

FIG. 14

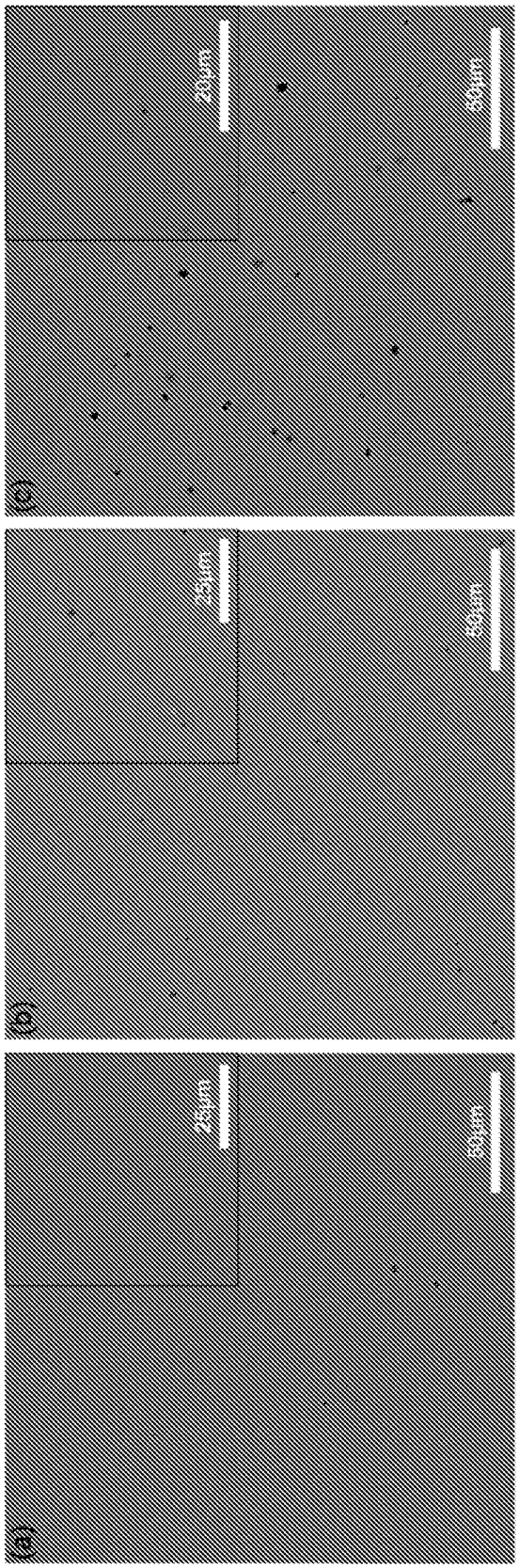

FIGS. 15A-15C

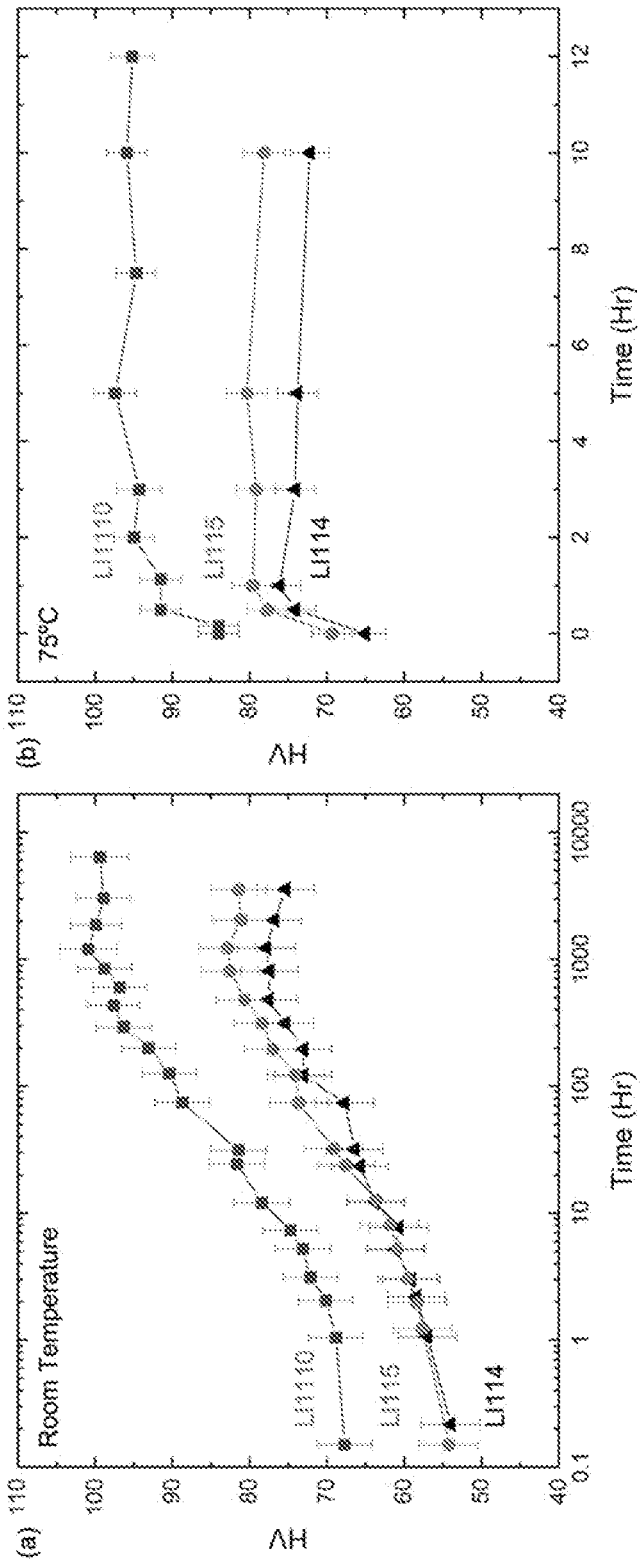
(a)
Room Temperature
HV
Time (Hr)
Li1110
Li115
Li114
(b)
75°C
HV
Time (Hr)
Li1110
Li115
Li114

FIGS. 16A-16B

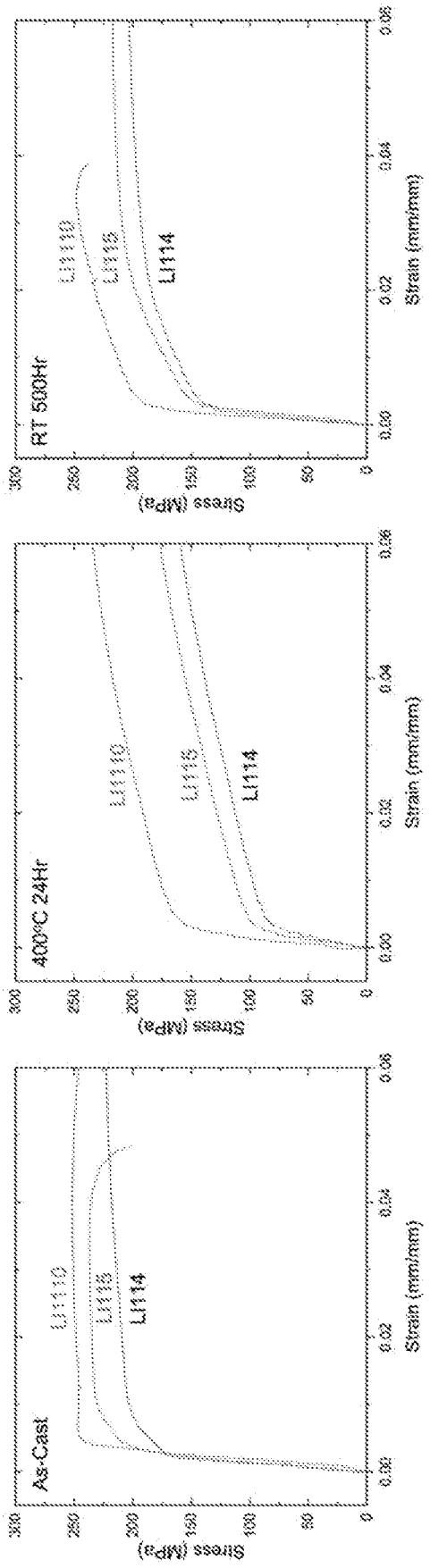
As-Cast
400°C 24Hr
RT 500Hr
LI1110
LI115
LI114
Stress (MPa)
Strain (mm/mm)

FIGS. 17A-17C

MAGNESIUM-LITHIUM ALLOYS COMPOSED OF GALLIUM OR INDIUM

CROSS-REFERENCE TO RELATED APPLICATIONS

[0001] This application claims the benefit of and priority to co-pending U.S. Provisional Patent Application No. 63/197,623, filed on Jun. 7, 2021, the contents of which are incorporated by reference herein in their entireties.

BACKGROUND

[0002] Magnesium (Mg) is the lightest structural metal with a density (1.74 g/cm^3) roughly a fifth of steel (7.87 g/cm^3) and two-thirds of aluminum (Al) (2.7 g/cm^3), which allows for significant reductions in weight [1]. In addition, Mg alloys have high specific strength and specific stiffness, good damping characteristics and superb castability and machinability [1], [2]. These outstanding properties combine to make Mg and its alloys promising materials of focus in automotive and aerospace applications. Additionally, in 2015, NASA standards were changed to allow the use of Mg in their designs [3]. One potential use for Mg is for lightweight shielding against micrometeorites [4]. This is necessary because medium sized fragments between 1 and 10 cm are not detectable from the ground but can cause catastrophic damage to satellites and spacecraft [5]. In this respect, both high strength and ductility are needed for a toughness high enough to be used as shielding material. However, Mg and its alloys have extremely limited fracture toughness, which is typically lower than that of Al alloys [6]. The poor fracture toughness is arising from their hexagonal close-packed (hcp) crystal structure, which has relatively few slip systems, and therefore results in a lower ductility [7].

[0003] The development of lightweight Mg—Li alloys was first investigated by NASA in the 1960s [4],[8]. These alloys were desired for their ultra-light weight and high ductility that results from the addition of Li [4]. Li possess a body center cubic (bcc) structure, which has significantly more slip systems than the hcp structure [4],[7]. Additionally, the lower density of Li (0.53 g/cm^3) will further lower the density of the Mg—Li alloy [4]. However, binary Mg—Li alloys possess yield and tensile strengths ranging from 60-110 MPa and 110-190 MPa, respectively, which is lower than desired or use in engineering applications [4], [9],[10].

[0004] In addition to lightweight effects, Mg—Li alloys can also provide radiation mitigation for deep space travel. This is a result of Mg and Li being low Z elements, which is beneficial against galactic cosmic rays (GCR) [11]. GCR interactions with high Z materials result in secondary radiation, which includes the production of secondary neutrons [12]. Neutrons can make up as much as 40% of the radiation a space crew experiences and are proven to have cancer causing effects [12]. Therefore, it is beneficial to develop alloys that can both reduce mass and provide radiation shielding properties for future space travel. Furthermore, the alloys need to possess increased strength and toughness.

SUMMARY

[0005] Described herein are Mg—Li alloys composed of gallium or indium. The amount of gallium or indium incorporated into the alloys enhances the physical properties of the alloys. For example, the addition of gallium or indium strengthens the alloys and makes them harder and tougher. In one aspect, the Mg—Li alloys described herein include gallium in the amount of from about 0.1 atomic percent to about 2 atomic percent or from about 0.5 weight percent to about 10 weight percent. In another aspect, the Mg—Li alloys described herein include indium in the amount of from about 0.1 atomic percent to about 2 atomic percent or from about 2 weight percent to about 15 weight percent. The alloys described herein have numerous applications where it is desirable to produce articles that are light-weight yet very strong and hard.

[0006] Other systems, methods, features, and advantages of the present disclosure will be or become apparent to one with skill in the art upon examination of the following drawings and detailed description. It is intended that all such additional systems, methods, features, and advantages be included within this description, be within the scope of the present disclosure, and be protected by the accompanying claims. In addition, all optional and preferred features and modifications of the described embodiments are usable in all aspects of the disclosure taught herein. Furthermore, the individual features of the dependent claims, as well as all optional and preferred features and modifications of the described embodiments are combinable and interchangeable with one another.

BRIEF DESCRIPTION OF THE DRAWINGS

[0007] Many aspects of the present disclosure can be better understood with reference to the following drawings. The components in the drawings are not necessarily to scale, emphasis instead being placed upon clearly illustrating the principles of the present disclosure. Moreover, in the drawings, like reference numerals designate corresponding parts throughout the several views.

[0008] FIGS. **1**A-**1**B show Vickers hardness measurements of (A) MgLiGa and (B) MgLiIn alloys that have been homogenized at 400° C. for 24 hours and aged in an oil bath at 75° C.

[0009] FIGS. **2**A-**2**C show representative SEM BSE images of three alloys in the as-cast state (a) LG122; (b) LG123; (c) LG125 alloys. All alloys exhibit a β matrix with α and $MgLi_2Ga$ phases.

[0010] FIG. **3** shows powder XRD data from three representative Mg—Li—Ga samples in the as-cast condition. Each alloy exhibits the β, α, and $MgLi_2Ga$ phases.

[0011] FIGS. **4**A-**4**C show representative SEM BSE images of all three alloys in the homogenized (400° C. 24 hours) state (a) LG122; (b) LG123; (c) LG125 alloys. All alloys exhibited a β matrix with a small degree of α-phase, but only the LG125 alloy exhibited the $MgLi_2Ga$ phase following homogenization.

[0012] FIG. **5** shows powder XRD data from three representative Mg—Li—Ga samples in the homogenized (400° C. 24 hr) condition.

[0013] FIG. **6** shows the comparison of room temperature aging characteristics for L12, LG122, LG123, LG125, and LA113 alloys as characterized by Vickers Hardness measurements.

[0014] FIGS. **7**A-**7**D show stress strain curves for tensile tests of the LG122, LG123, and LG124 alloys in the (a) as-cast; (b) homogenized 400° C. 24 hr; (c) room temperature aged for 24 hr; and (d) peak room temperature aged.

[0015] FIGS. **8**A-**8**F show SEM SE micrographs of tensile fracture surfaces for the as-cast alloys: (a) and (b) LG122 brittle cleavage fracture; (c) and (d) LG123 brittle cleavage fracture; (e) and (f) LG125 ductile fracture.

[0016] FIGS. **9**A-**9**F show SEM SE micrographs of fracture surfaces for alloys homogenized 400° C. 24 hr: (a) and (b) LG122 ductile fracture; (c) and (d) LG123 ductile fracture; (e) and (f) LG125 brittle cleavage fracture.

[0017] FIGS. **10**A-**10**F show SEM SE micrographs of fracture surfaces for alloys homogenized and room temperature aged 24 hr: (a) and (b) LG122 brittle cleavage fracture; (c) and (d) LG123 brittle cleavage fracture; (e) and (f) LG125 brittle intergranular/cleavage fracture.

[0018] FIGS. **11**A-**11**D show SEM SE micrographs of fracture surfaces for alloys homogenized and peak aged at room temperature: (a) and (b) LG122 aged 96 hr brittle intergranular fracture; (c) and (d) LG123 aged 72 hr brittle intergranular fracture.

[0019] FIGS. **12**A-**12**C show SEM BSE micrographs of as-cast (a) LI114; (b) LI115; (c) LI1110 alloys displaying a BCC matrix and MgLi2In phase in the grain boundaries.

[0020] FIGS. **13**A-**13**B show powder XRD patterns for LI114, LI115, and LI110 alloys in the (a) as-cast; (b) homogenized 400° C. 24 hr conditions.

[0021] FIG. **14** shows the SEM BSE micrograph of as-cast LI114 alloy displaying nano-scale In rich secondary phases within the BCC matrix.

[0022] FIGS. **15**A-**15**C show SEM BSE micrographs of (a) LI113; (b) LI115; (c) LI1110 homogenized 400° C. for 24 hr.

[0023] FIGS. **16**A-**16**B show Vickers hardness aging curves for LI114, LI115, and LI1110 aged at (a) room temperature and (b) 75° C. artificial aging.

[0024] FIGS. **17**A-**17**C show stress-strain curves for MgLiIn alloys loaded in uniaxial compression in the (a) as-cast; (b) 400° C. 24 hr; and (c) room temperature aged 500Hr. Plots include an inset of the LI115 alloy after testing.

DETAILED DESCRIPTION

[0025] Many modifications and other embodiments disclosed herein will come to mind to one skilled in the art to which the disclosed compositions and methods pertain having the benefit of the teachings presented in the foregoing descriptions and the associated drawings. Therefore, it is to be understood that the disclosures are not to be limited to the specific embodiments disclosed and that modifications and other embodiments are intended to be included within the scope of the appended claims. The skilled artisan will recognize many variants and adaptations of the aspects described herein. These variants and adaptations are intended to be included in the teachings of this disclosure and to be encompassed by the claims herein.

[0026] Although specific terms are employed herein, they are used in a generic and descriptive sense only and not for purposes of limitation.

[0027] As will be apparent to those of skill in the art upon reading this disclosure, each of the individual embodiments described and illustrated herein has discrete components and features which may be readily separated from or combined with the features of any of the other several embodiments without departing from the scope or spirit of the present disclosure.

[0028] Any recited method can be carried out in the order of events recited or in any other order that is logically possible. That is, unless otherwise expressly stated, it is in no way intended that any method or aspect set forth herein be construed as requiring that its steps be performed in a specific order. Accordingly, where a method claim does not specifically state in the claims or descriptions that the steps are to be limited to a specific order, it is no way intended that an order be inferred, in any respect. This holds for any possible non-express basis for interpretation, including matters of logic with respect to arrangement of steps or operational flow, plain meaning derived from grammatical organization or punctuation, or the number or type of aspects described in the specification.

[0029] All publications mentioned herein are incorporated herein by reference to disclose and describe the methods and/or materials in connection with which the publications are cited. The publications discussed herein are provided solely for their disclosure prior to the filing date of the present application. Nothing herein is to be construed as an admission that the present invention is not entitled to antedate such publication by virtue of prior invention. Further, the dates of publication provided herein can be different from the actual publication dates, which can require independent confirmation.

[0030] While aspects of the present disclosure can be described and claimed in a particular statutory class, such as the system statutory class, this is for convenience only and one of skill in the art will understand that each aspect of the present disclosure can be described and claimed in any statutory class.

[0031] It is also to be understood that the terminology used herein is for the purpose of describing particular aspects only and is not intended to be limiting. Unless defined otherwise, all technical and scientific terms used herein have the same meaning as commonly understood by one of ordinary skill in the art to which the disclosed compositions and methods belong. It will be further understood that terms, such as those defined in commonly used dictionaries, should be interpreted as having a meaning that is consistent with their meaning in the context of the specification and relevant art and should not be interpreted in an idealized or overly formal sense unless expressly defined herein.

[0032] Prior to describing the various aspects of the present disclosure, the following definitions are provided and should be used unless otherwise indicated. Additional terms may be defined elsewhere in the present disclosure.

Definitions

[0033] As used herein, "comprising" is to be interpreted as specifying the presence of the stated features, integers, steps, or components as referred to, but does not preclude the presence or addition of one or more features, integers, steps, or components, or groups thereof. Moreover, each of the terms "by", "comprising," "comprises", "comprised of," "including," "includes," "included," "involving," "involves," "involved," and "such as" are used in their open, non-limiting sense and may be used interchangeably. Further, the term "comprising" is intended to include examples and aspects encompassed by the terms "consisting essentially of" and "consisting of." Similarly, the term "consisting essentially of" is intended to include examples encompassed by the term "consisting of.

[0034] As used in the specification and the appended claims, the singular forms "a," "an" and "the" include plural referents unless the context clearly dictates otherwise. Thus,

for example, reference to "a metal," "a catalyst," or "a product," include, but are not limited to, combinations or mixtures of two or more such metals, catalysts, or products, and the like.

[0035] It should be noted that ratios, concentrations, amounts, and other numerical data can be expressed herein in a range format. It will be further understood that the endpoints of each of the ranges are significant both in relation to the other endpoint, and independently of the other endpoint. It is also understood that there are a number of values disclosed herein, and that each value is also herein disclosed as "about" that particular value in addition to the value itself. For example, if the value "10" is disclosed, then "about 10" is also disclosed. Ranges can be expressed herein as from "about" one particular value, and/or to "about" another particular value. Similarly, when values are expressed as approximations, by use of the antecedent "about," it will be understood that the particular value forms a further aspect. For example, if the value "about 10" is disclosed, then "10" is also disclosed.

[0036] When a range is expressed, a further aspect includes from the one particular value and/or to the other particular value. For example, where the stated range includes one or both of the limits, ranges excluding either or both of those included limits are also included in the disclosure, e.g. the phrase "x to y" includes the range from 'x' to 'y' as well as the range greater than 'x' and less than 'y'. The range can also be expressed as an upper limit, e.g. 'about x, y, z, or less' and should be interpreted to include the specific ranges of 'about x', 'about y', and 'about z' as well as the ranges of 'less than x', less than y', and 'less than z'. Likewise, the phrase 'about x, y, z, or greater' should be interpreted to include the specific ranges of 'about x', 'about y', and 'about z' as well as the ranges of 'greater than x', greater than y', and 'greater than z'. In addition, the phrase "about 'x' to 'y'", where 'x' and 'y' are numerical values, includes "about 'x' to about 'y'".

[0037] It is to be understood that such a range format is used for convenience and brevity, and thus, should be interpreted in a flexible manner to include not only the numerical values explicitly recited as the limits of the range, but also to include all the individual numerical values or sub-ranges encompassed within that range as if each numerical value and sub-range is explicitly recited. To illustrate, a numerical range of "about 0.1% to 5%" should be interpreted to include not only the explicitly recited values of about 0.1% to about 5%, but also include individual values (e.g., about 1%, about 2%, about 3%, and about 4%) and the sub-ranges (e.g., about 0.5% to about 1.1%; about 5% to about 2.4%; about 0.5% to about 3.2%, and about 0.5% to about 4.4%, and other possible sub-ranges) within the indicated range.

[0038] As used herein, the terms "about," "approximate," "at or about," and "substantially" mean that the amount or value in question can be the exact value or a value that provides equivalent results or effects as recited in the claims or taught herein. That is, it is understood that amounts, sizes, formulations, parameters, and other quantities and characteristics are not and need not be exact, but may be approximate and/or larger or smaller, as desired, reflecting tolerances, conversion factors, rounding off, measurement error and the like, and other factors known to those of skill in the art such that equivalent results or effects are obtained. In some circumstances, the value that provides equivalent results or effects cannot be reasonably determined. In such cases, it is generally understood, as used herein, that "about" and "at or about" mean the nominal value indicated±10% variation unless otherwise indicated or inferred. In general, an amount, size, formulation, parameter or other quantity or characteristic is "about," "approximate," or "at or about" whether or not expressly stated to be such. It is understood that where "about," "approximate," or "at or about" is used before a quantitative value, the parameter also includes the specific quantitative value itself, unless specifically stated otherwise.

[0039] As used herein, the terms "optional" or "optionally" means that the subsequently described event or circumstance can or cannot occur, and that the description includes instances where said event or circumstance occurs and instances where it does not.

[0040] As used herein, the term "admixing" is defined as mixing two or more components together so that there is no chemical reaction or physical interaction. The term "admixing" also includes the chemical reaction or physical interaction between the two or more components.

[0041] Described herein are Mg—Li alloys composed of gallium or indium. The amount of gallium or indium incorporated into the alloys enhances the physical properties of the alloys. For example, the addition of gallium or indium strengthens the alloys and makes them harder and tougher.

[0042] In one aspect, the Mg—Li alloys include gallium in the amount of from about 0.1 atomic percent to about 2 atomic percent, or about 0.1 atomic percent, 0.2 atomic percent, 0.3 atomic percent, 0.4 atomic percent, 0.5 atomic percent, 0.6 atomic percent, 0.7 atomic percent, 0.8 atomic percent, 0.9 atomic percent, 1.0 atomic percent, 1.1 atomic percent, 1.2 atomic percent, 1.3 atomic percent, 1.4 atomic percent, 1.5 atomic percent, 1.6 atomic percent, 1.7 atomic percent, 1.8 atomic percent, 1.9 atomic percent, or 2.0 atomic percent, where any value can be a lower and upper endpoint of a range (e.g., 0.2 atomic percent to 0.8 atomic percent, etc.).

[0043] In one aspect, the Mg—Li alloys include gallium in the amount of from about 0.5 weight percent to about 10 weight percent, or about 0.5 weight percent, 1.0 weight percent, 1.5 weight percent, 2.0 weight percent, 2.5 weight percent, 3.0 weight percent, 3.5 weight percent, 4.0 weight percent, 4.5 weight percent, 5.0 weight percent, 5.5 weight percent, 6.0 weight percent, 6.5 weight percent, 7.0 weight percent, 7.5 weight percent, 8.0 weight percent, 8.5 weight percent, 9.0 weight percent, 9.5 weight percent, or 10.0 weight percent, where any value can be a lower and upper endpoint of a range (e.g., 1.0 weight percent to 6.5 weight percent, etc.).

[0044] In one aspect, gallium is in the amount of from about 0.1 atomic percent to about 1.5 atomic percent. In another aspect, gallium is in the amount of from about 1 weight percent to about 5 weight percent.

[0045] In one aspect, the Mg—Li alloys include indium in the amount of from about 0.1 atomic percent to about 2 atomic percent, or about 0.1 atomic percent, 0.2 atomic percent, 0.3 atomic percent, 0.4 atomic percent, 0.5 atomic percent, 0.6 atomic percent, 0.7 atomic percent, 0.8 atomic percent, 0.9 atomic percent, 1.0 atomic percent, 1.1 atomic percent, 1.2 atomic percent, 1.3 atomic percent, 1.4 atomic percent, 1.5 atomic percent, 1.6 atomic percent, 1.7 atomic percent, 1.8 atomic percent, 1.9 atomic percent, or 2.0

atomic percent, where any value can be a lower and upper endpoint of a range (e.g., 0.2 atomic percent to 0.8 atomic percent, etc.).

[0046] In one aspect, the Mg—Li alloys include indium in the amount of from about 2.0 weight percent to about 15 weight percent, or about 2.0 weight percent, 2.5 weight percent, 3.0 weight percent, 3.5 weight percent, 4.0 weight percent, 4.5 weight percent, 5.0 weight percent, 5.5 weight percent, 6.0 weight percent, 6.5 weight percent, 7.0 weight percent, 7.5 weight percent, 8.0 weight percent, 8.5 weight percent, 9.0 weight percent, 9.5 weight percent, 10.0 weight percent, 10.5 weight percent, 11.0 weight percent, 11.5 weight percent, 12.0 weight percent, 12.5 weight percent, 13.0 weight percent, 13.5 weight percent, 14.0 weight percent, 14.5 weight percent, or 15.0 weight percent, where any value can be a lower and upper endpoint of a range (e.g., 4.0 weight percent to 10.0 weight percent, etc.).

[0047] In one aspect, indium is in the amount of from about 0.5 atomic percent to about 2 atomic percent. In another aspect, indium is in the amount of from about 2 weight percent to about 10 weight percent.

[0048] In one aspect, the amount of lithium in the alloys described herein is from about 23 atomic percent to about 35 atomic percent, or about 23 atomic percent, 23.5 atomic percent, 24 atomic percent, 24.5 atomic percent, 25 atomic percent, 25.5 atomic percent, 26 atomic percent, 26.5 atomic percent, 27 atomic percent, 27.5 atomic percent, 28 atomic percent, 28.5 atomic percent, 29 atomic percent, 29.5 atomic percent, 30 atomic percent, 30.5 atomic percent, 31 atomic percent, 31.5 atomic percent, 32 atomic percent, 32.5 atomic percent, 33 atomic percent, 33.5 atomic percent, 34 atomic percent, 34.5 atomic percent, or 35 atomic percent, where any value can be a lower and upper endpoint of a range (e.g., 30 atomic percent to 32 atomic percent, etc.).

[0049] In one aspect, the amount of lithium in the alloys described herein is from about 8.0 weight percent to about 15 weight percent, or about 8.0 weight percent, 8.5 weight percent, 9.0 weight percent, 9.5 weight percent, 10.0 weight percent, 10.5 weight percent, 11.0 weight percent, 11.5 weight percent, 12.0 weight percent, 12.5 weight percent, 13.0 weight percent, 13.5 weight percent, 14.0 weight percent, 14.5 weight percent, or 15.0 weight percent, where any value can be a lower and upper endpoint of a range (e.g., 10.0 weight percent to 11.5 weight percent, etc.).

[0050] In one aspect, lithium is in the amount of from about 30 atomic percent to about 31 atomic percent. In another aspect, lithium is in the amount of from about 10 weight percent to about 12 weight percent.

[0051] In one aspect, gallium is in the amount of from about 0.1 atomic percent to about 1.5 atomic percent and lithium is in the amount of from about 30 atomic percent to about 31 atomic percent. In another aspect, gallium is in the amount of from about 1 weight percent to about 5 weight percent and lithium is in the amount of from about 10 weight percent to about 12 weight percent.

[0052] In one aspect, indium is in the amount of from about 0.5 atomic percent to about 2 atomic percent and lithium is in the amount of from about 30 atomic percent to about 31 atomic percent. In another aspect, indium is in the amount of from about 2 weight percent to about 10 weight percent and lithium is in the amount of from about 10 weight percent to about 12 weight percent.

[0053] The balance of the alloys described herein include magnesium. For example, if the MgLiGa alloy includes 30 atomic percent lithium and 1.5 atomic percent gallium, the alloy includes 68.5 atomic percent magnesium.

[0054] The alloys described herein have numerous applications where it is desirable to produce articles that are light-weight yet very strong and hard. In one aspect, the alloys described herein have a Vickers hardness of from about 70 HV to about 120 HV, or about 70 HV, 75 HV, 80 HV, 85 HV, 90 HV, 95 HV, 100 HV, 105 HV, 110 HV, 115 HV, or 120 HV, where any value can be a lower and upper endpoint of a range (e.g., 75 HV to 110 HV, etc.).

[0055] In one aspect, the alloys described herein have a yield strength (YS) of from about 100 MPa to about 350 MPa, or about 100 MPa, 125 MPa, 150 MPa, 175 MPa, 200 MPa, 225 MPa, 250 MPa, 275 MPa, 300 MPa, 325 MPa, or 350 MPa, where any value can be a lower and upper endpoint of a range (e.g., 125 MPa to 325 MPa, etc.).

[0056] In one aspect, the alloys described herein have an ultimate tensile strength (UTS) of from about 100 MPa to about 350 MPa, or about 100 MPa, 125 MPa, 150 MPa, 175 MPa, 200 MPa, 225 MPa, 250 MPa, 275 MPa, 300 MPa, 325 MPa, or 350 MPa, where any value can be a lower and upper endpoint of a range (e.g., 125 MPa to 325 MPa, etc.).

[0057] In one aspect, the alloys described herein have a percent elongation of from about 0.5 percent to about 25 percent, or about 0.5 percent, 1.0 percent, 2.5 percent, 5.0 percent, 7.5 percent, 10.0 percent, 12.5 percent, 15.0 percent, 17.5 percent, 20.0 percent, 22.5 percent, or 25.0 percent, where any value can be a lower and upper endpoint of a range (e.g., 2.5 percent to 17.5 percent, etc.).

[0058] The alloys described herein are predominantly a body-centered cubic (BCC) phase as determined by X-ray powder diffraction. In one aspect, the alloy is at least 50%, at least 55%, at least 60%, at least 65%, at least 70%, at least 75%, at least 80%, at least 85%, at least 90%, or at least 95% a body-centered cubic (BCC) phase. In another aspect, the alloy is predominantly a body-centered cubic (BCC) phase with a face-centered cubic (FCC) based phase as determined by powder X-ray diffraction, the BCC phase is greater than 50%, greater than 60%, greater than 70%, greater than 80%, greater than 90%, or greater than 95%. In another aspect, the alloy has a BCC phase from greater than 50% up to 100% of the alloy as determined by powder X-ray diffraction, or greater than 50%, 55%, 60%, 65%, 70%, 75%, 80%, 85%, 90%, 95%, or up to 100%, where any value can be a lower and upper endpoint of a range (e.g., 60% to 85%, etc.).

[0059] In one aspect, the alloy has an X-ray powder diffraction pattern comprising a peak at 36.0°±0.2° 2θ as measured by X-ray powder diffraction using an x-ray wavelength of 1.54 Å. In another aspect, the alloy has an X-ray powder diffraction pattern comprising peaks at 36.0° and 52.0°±0.2° 2θ as measured by X-ray powder diffraction using an x-ray wavelength of 1.54 Å. In another aspect, the alloy has an X-ray powder diffraction pattern comprising peaks at 36.0°, 52.0°, and 64.9°±0.2° 2θ as measured by X-ray powder diffraction using an x-ray wavelength of 1.54 Å. In another aspect, the alloy has an X-ray powder diffraction pattern comprising peaks at 36.0°, 52.0°, 64.9°, and 76.7°±0.2° 2θ as measured by X-ray powder diffraction using an x-ray wavelength of 1.54 Å.

[0060] In one aspect, the alloy has an X-ray powder diffraction pattern comprising of body-centered cubic (BCC) peaks at about 36.3°, 52.2°, 65.1°, and 76.7°±0.2° 2θ as measured by X-ray powder diffraction using an x-ray wavelength of 1.54 Å.

[0061] In one aspect, the alloy has an X-ray powder diffraction pattern comprising $MgLi_2Ga$ face-centered cubic (FCC) based peaks at 23.3°, 27.0°, 38.5°, 45.5°, and 55.6°±0.2° 2θ as measured by X-ray powder diffraction using an x-ray wavelength of 1.54 Å.

[0062] In one aspect, the alloy has an X-ray powder diffraction pattern comprising $MgLi_2In$ face-centered cubic (FCC) based peaks at about 22.3°, 25.8°, 36.8°, and 43.5°±0.2° 2θ as measured by X-ray powder diffraction using an x-ray wavelength of 1.54 Å.

[0063] In one aspect, the alloy has an X-ray powder diffraction pattern comprising hexagonal close-packed (HCP) peaks at 32.2°, 34.9°, 36.8°, 48.2°, 57.5°, 63.6°, and 69.1°±0.2° 2θ as measured by X-ray powder diffraction using an x-ray wavelength of 1.54 Å.

[0064] In one aspect, the alloys described herein are produced by the process comprising

[0065] (a) melting magnesium, lithium, and gallium or indium to produce a first composition;

[0066] (b) homogenizing the first composition to produce a predominately body-centered cubic (BCC) structure; and

[0067] (c) ageing the body-centered cubic (BCC) structure to produce the alloy.

[0068] The first step involves admixing the melting magnesium, lithium, and gallium or indium at a temperature of from about 700° C. to 800° C., or about 700° C., 725° C., 750° C., 775° C., or 800° C., where any value can be a lower and upper endpoint of a range (e.g., 725° C. to 750° C., etc.). The melting step can be performed under an inert atmosphere. After melting step (a), the sample is homogenized by heating the sample at a temperature of from about 300° C. to 500° C., or about 300° C., 350° C., 400° C., 450° C., or 500° C., where any value can be a lower and upper endpoint of a range (e.g., 350° C. to 450° C., etc.). After homogenization, the sample is aged by heating the sample at from 21° C. to 100° C. followed by cooling to room temperature. Non-limiting procedures for making the alloys described herein are provided in the Examples.

Aspects

[0069] Aspect 1: An alloy comprising

[0070] (a) gallium in the amount of from about 0.1 atomic percent to about 2 atomic percent or from about 0.5 weight percent to about 10 weight percent;

[0071] (b) lithium in the amount of from about 23 atomic percent to about 35 atomic percent or from about 8 weight percent to about 15 weight percent; and

[0072] (c) the balance of the alloy is magnesium.

[0073] Aspect 2: The alloy of Aspect 1, wherein gallium is in the amount of from about 0.1 atomic percent to about 2 atomic percent.

[0074] Aspect 3: The alloy of Aspect 1, wherein gallium is in the amount of from about 1 weight percent to about 5 weight percent.

[0075] Aspect 4: The alloy of Aspect 1, wherein lithium is in the amount of from about 23 atomic percent to about 31 atomic percent.

[0076] Aspect 5: The alloy of Aspect 1, wherein lithium is in the amount of from about 8 weight percent to about 12 weight percent.

[0077] Aspect 6: The alloy of Aspect1, wherein gallium is in the amount of from about 0.1 atomic percent to about 1.5 atomic percent and lithium is in the amount of from about 23 atomic percent to about 31 atomic percent.

[0078] Aspect 7: The alloy of Aspect 1, wherein gallium is in the amount of from about 1 weight percent to about 5 weight percent and lithium is in the amount of from about 8 weight percent to about 12 weight percent.

[0079] Aspect 8: An alloy comprising

[0080] (a) indium in the amount of from about 0.1 atomic percent to about 2 atomic percent or from about 2 weight percent to about 15 weight percent;

[0081] (b) lithium in the amount of from about 23 atomic percent to about 35 atomic percent or from about 10 weight percent to about 15 weight percent; and

[0082] (c) the balance of the alloy is magnesium.

[0083] Aspect 9: The alloy of Aspect 8, wherein indium is in the amount of from about 0.5 atomic percent to about 2 atomic percent.

[0084] Aspect 10: The alloy of Aspect 8, wherein indium is in the amount of from about 2 weight percent to about 10 weight percent.

[0085] Aspect 11: The alloy of Aspect 8, wherein lithium is in the amount of from about 23 atomic percent to about 31 atomic percent.

[0086] Aspect 12: The alloy of Aspect 8, wherein lithium is in the amount of from about 8 weight percent to about 12 weight percent.

[0087] Aspect 13: The alloy of Aspect 8, wherein indium is in the amount of from about 0.5 atomic percent to about 2 atomic percent and lithium is in the amount of from about 23 atomic percent to about 31 atomic percent.

[0088] Aspect 14: The alloy of Aspect 8, wherein indium is in the amount of from about 2 weight percent to about 10 weight percent and lithium is in the amount of from about 8 weight percent to about 12 weight percent.

[0089] Aspect 15: The alloy in any one of Aspects 1 to 14, wherein the alloy has a Vickers hardness of from about 70 HV to about 120 HV.

[0090] Aspect 16: The alloy in any one of Aspects 1 to 14, wherein the alloy has a yield strength (YS) of from about 100 MPa to about 350 MPa.

[0091] Aspect 17: The alloy in any one of Aspects 1 to 14, wherein the alloy has an ultimate tensile strength (UTS) of from about 100 MPa to about 350 MPa.

[0092] Aspect 18: The alloy in any one of Aspects 1 to 14, wherein the alloy has a percent elongation of from about 0.5 percent to about 25 percent.

[0093] Aspect 19: The alloy of any one of Aspects 1 to 14, wherein the alloy is predominantly a body-centered cubic (BCC) phase as determined by powder X-ray diffraction.

[0094] Aspect 20: The alloy of any one of Aspects 1 to 14, wherein the alloy is predominantly a body-centered cubic (BCC) phase with a face-centered cubic (FCC) based phase as determined by X-ray powder diffraction.

[0095] Aspect 21: The alloy of any one of Aspects 1 to 14, wherein the alloy has an X-ray powder diffraction pattern comprising of body-centered cubic (BCC) peaks at about 36.3°, 52.2°, 65.1°, and 76.7°±0.2° 20 as measured by X-ray powder diffraction using an x-ray wavelength of 1.54 Å.

[0096] Aspect 22: The alloy of any one of Aspects 1 to 14, wherein the alloy has an X-ray powder diffraction pattern comprising $MgLi_2Ga$ face-centered cubic (FCC) based

peaks at 23.3°, 27.0°, 38.5°, 45.5°, and 55.6°±0.2° 2θ as measured by X-ray powder diffraction using an x-ray wavelength of 1.54 Å.

[0097] Aspect 23: The alloy of any one of Aspects 1 to 14, wherein the alloy has an X-ray powder diffraction pattern comprising $MgLi_2In$ face-centered cubic (FCC) based peaks at about 22.3°, 25.8°, 36.8°, and 43.5°±0.2° 2θ as measured by X-ray powder diffraction using an x-ray wavelength of 1.54 Å.

[0098] Aspect 24: The alloy of any one of Aspects 1 to 14, wherein the alloy has an X-ray powder diffraction pattern comprising hexagonal close-packed (HCP) peaks at 32.2°, 34.9°, 36.8°, 48.2°, 57.5°, 63.6°, and 69.1°±0.2° 2θ as measured by X-ray powder diffraction using an x-ray wavelength of 1.54 Å.

[0099] Aspect 25: The alloy of any one of Aspects 1 to 24, wherein the alloy is produced by the process comprising

[0100] (a) melting magnesium, lithium, and gallium or indium to produce a first composition;

[0101] (b) homogenizing the first composition to produce a predominately body-centered cubic (BCC) structure; and

[0102] (c) ageing the body-centered cubic (BCC) structure to produce the alloy.

[0103] Aspect 26: The alloy of Aspect 25, wherein in step (a) the magnesium, lithium, and gallium or indium are mixed with one another at a temperature of from about 700° C. to about 800° C.

[0104] Aspect 27: The alloy of Aspect 25 or 26, wherein in step (b), the first composition is heated at a temperature of from about 300° C. to about 500° C. from about 1 hour to about 48 hours.

[0105] Aspect 28: The alloy of any one of Aspects 25 to 27, wherein in step (c), the body-centered cubic (BCC) structure is aged at a temperature of from about 25° C. to about 100° C.

[0106] Aspect 29: An article comprising the alloy of any one of claims **1** to **28**.

[0107] Aspect 30: The article of Aspect 29, wherein the article is to be used in space travel.

[0108] Now having described the aspects of the present disclosure, in general, the following Examples describe some additional aspects of the present disclosure. While aspects of the present disclosure are described in connection with the following examples and the corresponding text and figures, there is no intent to limit aspects of the present disclosure to this description. On the contrary, the intent is to cover all alternatives, modifications, and equivalents included within the spirit and scope of the present disclosure.

EXAMPLES

[0109] The following examples are put forth so as to provide those of ordinary skill in the art with a complete disclosure and description of how the compounds, compositions, articles, devices and/or methods claimed herein are made and evaluated, and are intended to be purely exemplary of the disclosure and are not intended to limit the scope of what the inventors regard as their disclosure. Efforts have been made to ensure accuracy with respect to numbers (e.g., amounts, temperature, etc.), but some errors and deviations should be accounted for. Unless indicated otherwise, parts are parts by weight, temperature is in ° C. or is at ambient temperature, and pressure is at or near atmospheric.

Example 1

Experimental Procedures and Characterization

[0110] Alloys were cast using Mg granules (99.8 pct metal basis), Li shot (99 pct metal basis), and Ga (99.99 pct). Samples were cast using a resistance furnace within a MBraun Labstar Glovebox with a positive pressure argon (Ar) atmosphere (<30 ppm O2). Melting was performed at 750° C. in a stainless-steel crucible that was covered with a graphite lid. Raw metals were melted for 20 min, followed by three stirs 5 min apart using a graphite stir rod. Following the third stir, the molten metal was poured into a graphite mold. To avoid contamination, the stainless-steel crucible, graphite stir rod, and graphite mold were coated with aerosol boron nitride and allowed to dry in a fume hood prior to use. Compositions of cast alloys are displayed in Table 1.

TABLE 1

Alloy compositions measured via ICP-OES and nomenclature for alloys

Alloy	Mg at %	Li at %/ wt %	Ga at %/ wt %	In at %/ wt %
LG1	Balance	30.8/11.2	0.3/1.2	—
LG2	Balance	30.9/11.0	1.3/4.6	—
LG3	Balance	30.5/10.7	1.7/6.0	—
LI1	Balance	31.4/11.2	—	0.7/4.1
LI2	Balance	31.9/11.3	—	0.9/5.3
LI3	Balance	31.5/11.8	—	1.8/10.2

[0111] Homogenization heat treatments were performed on samples encapsulated in a Pyrex tube. Before inserting the samples into the Pyrex tube, all surface oxide was removed with 600 grit SiC paper, samples were ultrasonicated in isopropanol for 5 minutes and wrapped in 306 stainless steel foil. Encapsulation involved pulling a vacuum to ≤35 millitorr and backfilling to ~400 torr with ultra-high-purity Ar (99.999%) before sealing with a hydrogen torch. Homogenization was performed at 400° C. for 24 hours. Following homogenization, samples were quenched in water followed by sectioning into pieces roughly 1×1×3 mm with a low speed saw and aged in an oil bath at 75° C. Samples were cooled to room temperature in air followed by mounting in epoxy. Vickers hardness testing was performed on the aged samples that were mounted in epoxy and polished to a 1 μm finish. A Wilson Hardness tester was used with a load of 100 grams and hold time of 10 seconds.

[0112] X-ray diffraction (XRD) was used to identify phases present within the alloys. Powder samples were made by filing bulk samples. A Cu Kα x-ray beam was used with a current of 40 mA and voltage of 45 kV. The scan was performed in the 2 theta scan range of 20-80° with a step size of 0.008° and a dwell time of 15 seconds per step. Table 2 provides the XRD peaks with corresponding phases for the MgLiGa and MgLiIn alloys.

TABLE 2

MgLiGa	Phase	MgLiIn	Phase
23.3°	MgLi2Ga	22.3°	MgLi2In
27.0°	MgLi2Ga	25.8°	MgLi2In
32.3°	HCP	32.2°	HCP
34.9°	HCP	34.7°	HCP
36.0°	BCC	36.1°	BCC

TABLE 2-continued

MgLiGa	Phase	MgLiln	Phase
36.8°	HCP	36.8°	MgLi2In
38.5°	MgLi2Ga	36.8°	HCP
45.5°	MgLi2Ga	43.5°	MgLi2In
48.2°	HCP	45.6°	MgLi2In
52.0°	BCC	48.2°	HCP
55.6°	MgLi2Ga	52.0°	BCC
57.7°	HCP	57.3°	HCP
63.9°	HCP	58.3°	MgLi2In
64.9°	BCC	63.6°	HCP
69.2°	HCP	64.9°	BCC
76.8°	BCC	66.4°	MgLi2In
		69.0°	HCP
		76.6°	BCC

[0113] FIGS. **1**A and **1**B show Vickers hardness measurement of MgLiGa and MgLiIn alloys from Table 1. It can be seen in FIG. **1**A that an increase from 1.3 at % to 1.7 at % Ga did not correspond to any increase in strength. Therefore, no further additions are explored. In the MgLiIn alloys, it was observed that the LI3 had deformation surrounding the hardness indentations (FIG. **1**B), which is believed to indicate a transition to a more brittle material. Therefore, greater In additions will likely further embrittle the material.

REFERENCES FOR EXAMPLE 1

[0114] [1] Ye, Hai Zhi, and Xing Yang Liu. "Review of Recent Studies in Magnesium Matrix Composites." Journal of Materials Science, vol. 39, no. 20, 2004, pp. 6153-6171.

[0115] [2] Somekawa, Hidetoshi, and Toshiji Mukai. "Effect of Texture on Fracture Toughness in Extruded AZ31 Magnesium Alloy." Scripta Materialia, vol. 53, no. 5, 2005, pp. 541-545.

[0116] [3] National Aeronautics and Space Administration. Standard Materials and Processes Requirements for Spacecraft. Tech. Print. NASA-STD-6016 [4] Frost, P. D. Magnesium-Lithium Alloys: A Review of Current Developments. Defense Metals Information Center.

[0117] [5] Tanaka, Makoto, et al. "Development of a Lightweight Space Debris Shield Using High Strength Fibers." International Journal of Impact Engineering, vol. 26, no. 1-10, 2001, pp. 761-772.

[0118] [6] Somekawa, Hidetoshi, et al. "High Fracture Toughness of Extruded Mg—Zn—Y Alloy by the Synergistic Effect of Grain Refinement and Dispersion of Quasicrystalline Phase." Scripta Materialia, vol. 56, no. 12, 2007, pp. 1091-1094.

[0119] [7] Callister, William D. Jr., and David G. Rethwisch. Fundamentals of Materials Science and Engineering an Integrated Approach. Wiley, 2012.

[0120] [8] Bryrer, T. G. The Development of Magnesium-Lithium Alloys for Structural Applications. National Aeronautics and Space Administration.

[0121] [9] Park, Gyu Hyeon, et al. "Development of Lightweight MgLiAl Alloys with High Specific Strength." Journal of Alloys and Compounds, vol. 680, 2016, pp. 116-120.

[0122] Lee, R. E., and W. J. D. Jones. "Microplasticity and Fatigue of Some Magnesium-Lithium Alloys." Journal of Materials Science, vol. 9, no. 3, 1974, pp. 469-475.

[0123] Rojdev, Kristina, and William Atwell. "46th International Conference on Environmental Systems." Investigation of Lithium Metal Hydride Materials for Mitigation of Deep Space Radiation.

[0124] Mcphee, Jacey C, and John B Charles. "Human Health and Performance Risks of Space Exploration Missions." National Aeronautics and Space Administration, humanresearchroadmap.nasa.gov/evidence/reports/EvidenceBook.pdf.

Example 2

Experimental Procedures

Sample Preparation

[0125] Alloys were fabricated using Mg (99.8 wt % Alfa Aesar), Li (99 wt % Sigma Aldrich), and Ga (99.99 wt % Gallium Source). Samples were cast using a resistance furnace within a MBraun Labstar Glovebox with a positive pressure argon (Ar) atmosphere (<30 ppm O2). Melting was performed at 750° C. in a boron nitride coated stainless-steel crucible that was covered with a graphite lid. Raw metals were melted for 20 min followed by three stirs 5 minutes apart, and then poured into a boron nitride coated graphite mold. Alloys with 12 wt % Li and varying Ga content were cast for analysis. The 12 wt % Li was chosen to maintain a β-phase matrix while accounting for compositional tolerance during casting. Ga content of 2, 3, and 5 wt % (denoted LG122, LG123, and LG125, respectively) were chosen to detail the strengthening effects throughout the solubility region of this system. Nominal compositions of alloys are displayed in Table 3.

TABLE 3

Nominal Mg—Li—Ga alloy compositions.

Alloy	Mg at %	Li wt % (at %)	Ga wt % (at %)
LG122	Balance	12 (33)	2 (0.5)
LG123	Balance	12 (33)	3 (0.9)
LG125	Balance	12 (33)	5 (1.2)

[0126] For homogenization heat treatments, samples were encapsulated in Pyrex tubes under ultra-high-purity Ar (99.999 wt %). Prior to encapsulation, samples were ground with 600 grit SiC paper to remove surface oxidation, ultrasonically cleaned in isopropanol for 5 minutes, and wrapped in 304 stainless steel foil to avoid contact with the tube. A vacuum was pulled to ≤0.035 torr followed by backfilling to ~400 torr with Ar before sealing. Backfilling was performed to avoid Mg vaporization during heat treatment. Samples were homogenized at 400° C. for 24 hours prior to quenching in water.

Sample Characterization

[0127] Microstructural characteristics of these alloys were investigated utilizing a Tescan Mira scanning electron microscope (SEM). Powder XRD with a Panalytical XPert Powder system was used to identify phases present within the alloys. Powder samples were made by filing bulk samples. Homogenized samples were analyzed within 30 minutes of quenching. A Cu Kα x-ray beam was used with a 2 theta scan range of 20-80°, step size of 0.008°, and dwell time of 15 seconds per step. Rietveld refinement was

performed utilizing the open source GSAS II code to calculate lattice parameters and phase fractions from powder patterns [14].

Mechanical Properties

[0128] Room temperature aging trials involved recording Vickers hardness measurements on homogenized samples. Hardness measurements were taken on a Wilson Vickers Hardness tester with 100 grams force and 10s hold time. Five hardness measurements were taken for each data point and error bars are reflective of uncertainty as determined by practices outlined in ASTM E92 [15]. Tensile testing was performed using an Instron 3119 load frame. Dog bones were cast using the same procedure listed before and sectioned 1.5 mm thick. A strain rate of 10^{-3} s^{-1} was utilized for all tension tests.

Results

Alloy Microstructure

[0129] As cast SEM BSE micrographs of the three alloys are displayed in FIG. **2**. These micrographs display a β-phase matrix with a and $MgLi_2Ga$ phases distributed within the matrix and $MgLi_2Ga$ phase located in the grain boundaries for all three alloys. XRD in FIG. **3** confirms the identification of the phases present within each alloy to be the β, α, and $MgLi_2Ga$ phases. With greater Ga additions, the phase fraction of $MgLi_2Ga$ increased with values of 2.0, 4.6, and 6.8% for the LG122, LG123, and LG125 alloys, respectively. The presence of the α-phase followed the same trend with values of 2.9, 5.9, and 6.4% for the LG122, LG123, and LG125 alloys, respectively.

[0130] Micrographs of the LG122, LG123, and LG125 alloys homogenized 400° C. for 24 hours are displayed in FIG. **4**. Following homogenization, only the LG125 alloy exhibited the $MgLi_2Ga$ phase. These secondary phases were residual from the casting process and are indicative of this alloy containing a greater Ga content than what is soluble in the β matrix at 400° C. The XRD patterns in FIG. **5** confirm that the LG125 alloy possessed 1.5% of the $MgLi_2Ga$ phase following homogenization while the LG122 and LG123 are composed of the β matrix and a small degree of α-phase.

Room Temperature Aging Trials

[0131] The Mg—Li—Ga alloys exhibit room temperature aging effects, similar to the Mg—Li—Al system [2,7]. A description of room temperature aging of the LG122, LG123, and LG125 alloys is displayed using hardness measurements in FIG. **6**. This plot includes the binary Mg-12 wt % Li alloy (L12) to display the strengthening contribution of Ga additions. The L12 alloy exhibits no room temperature hardness evolution. The Mg-11Li-3Al (LA113) alloy was also cast for comparison since it is a commonly tested high strength Mg—Li—Al alloy [6,7]. From this comparison, it is seen that the LA113 alloy exhibits a higher initial strength than the Mg—Li—Ga alloys. However, little precipitation hardening takes place following the quench before overaging occurred due to the high Al content and sizeable lattice mismatch of the Mg_3Al phase with the β matrix (−3.3%) [7].

[0132] It is observed that there is an increase in hardening effects as the Ga content is increased. Initially, this is likely due to an increased supersaturation of the matrix resulting in increased solid solution strengthening effects. Additionally, the higher degree of supersaturation increases the driving force for precipitate nucleation/growth thereby increasing precipitation strengthening effects as these alloys age. However, this increase in Ga content typically also increases the rate of overaging due to a transition from dislocation shearing to bowing at a smaller average precipitate radius [16]. The LG122, LG123, and LG125 alloys overaged at 615, 800, and 530 Hr respectively. Overaging was characterized as a 5% decrease in peak hardness. It is interesting to note that the LG123 alloy exhibited a greater resistance to overaging than the LG122 alloy.

Mechanical Properties—Tension Tests

[0133] Tensile tests performed on the as-cast LG122, LG123, and LG125 alloys are displayed in FIG. **9***a*. Yield strength (YS), ultimate tensile strength (UTS), and elongation (Elong) values for these tests are summarized in Table 3. It is observed that the as-cast strength values are very similar between the three compositions. However, the LG125 alloy exhibited a significantly greater ductility than the lower Ga containing alloys. Fracture surfaces of these alloys are summarized in FIG. **10**. It is observed that the lower Ga containing alloys exhibited brittle intergranular fracture with a combination of microvoid coalescence at the grain boundaries and cleavage fracture. In contrast, the LG125 alloy exhibited a more ductile fracture with the formation of dimples and tear ridges.

[0134] Results in FIG. **9***b* display that upon homogenization, the YS and UTS of the LG123 and LG125 alloys increased while the YS of the LG122 alloy is decreased. The increase in strength is likely due in part to solid solution strengthening effects. It was observed that the LG122 and LG123 alloys exhibited a significant increase in ductility upon homogenization. FIG. **11** displays that the fracture mechanism for these alloys changed to a ductile dimple fracture. This is likely due to the dissolution of secondary phases that act as crack initiation sites in the as-cast state. Conversely, the LG125 alloy transitioned from ductile to brittle fracture upon homogenization. This alloy exhibited a combination of cleavage fracture and particle nucleated dimples.

[0135] FIGS. **9***c* and **9***d* show that significant strength increases occurred upon room temperature aging. Following 24 hours of room temperature aging, the LG122, LG123, LG125 alloys exhibited increases in strength of 95, 43, and 47%, respectively from the homogenized state. This is indicative of precipitation strengthening within these alloys. However, this increase in strength was at a cost of ductility. FIG. **10** displays that the LG122 and LG123 alloys failed via cleavage fracture. The LG125 alloy failed through a combination of cleavage and intergranular fracture. Secondary phases resided on both the cleavage planes and grain boundaries of this alloy.

[0136] Further aging of the LG122 and LG123 to their peak precipitation hardened points (determined from hardness trials in FIG. **6**) displayed that these alloys continued to strengthen. In the peak room temperature aged state, the YS values increased 132 and 71% from the homogenized state for the LG122 and LG123 alloys, respectively. With this further increase in strength, the fracture mechanism changed to a predominantly intergranular fracture with the formation of some cleavage planes as seen in FIG. **11**.

[0137] The room temperature aged alloys exhibited serrated flow near the yield strength. The cause of these serrations is unclear, but their presence is dependent on the precipitates that strengthen this system as seen by their absence in the homogenized samples and occurrence in the high strength aged samples.

TABLE 4

Summary of mechanical testing data and corresponding grain sizes of alloys.

Alloy		YS (MPa)	UTS (MPa)	Elong (%)	Grain Size (μm)
LG122	As Cast	130	131	0.8	372 ± 74
	400° C. 24 Hr	88	134	20	496 ± 89
	RT 24 Hr	172	195	6.7	
	RT 96 Hr	204	217	5.3	
LG123	As Cast	121	123	1.1	170 ± 33
	400° C. 24 Hr	136	180	18	
	RT 24 Hr	237	243	1.6	204 ± 42
	RT 72 Hr	232	233	1.4	
LG125	As Cast	122	138	15	180 ± 23
	400° C. 24 Hr	196	198	1.0	192 ± 46
	RT 24 Hr	289	289	1.2	

DISCUSSION

[0138] The coarsening rates of the Mg—Li—Ga system were shown to be slower than that of the Mg—Li—Al system [7]. Coarsening rates follow the relationship:

$$k \propto D\gamma \tag{1}$$

[0139] Where k is an alloy specific coarsening rate for a given temperature, D is the diffusion coefficient and γ is the interfacial energy [16]. The diffusion coefficients of both Al and Ga have not been assessed yet within the β Mg—Li system therefore it is not possible to compare this term at this time. The γ term is correlated to the lattice mismatch between the precipitate and matrix phases. The calculated lattice parameters of the β-phase matrix and $MgLi_2Ga$ phase from the XRD measurements in FIG. **5** are 3.51 and 6.61 Å, respectively. Assuming the "cube on cube" alignment typical of this structure within a ß-phase matrix [7], the calculation of interphase misfit follows the relation

$$\delta = \frac{a_{MgLi2Ga} - 2a_{BCC}}{2a_{BCC}} \times 100 \tag{2}$$

[0140] Therefore, there is a lattice mismatch of −5.8% between the $MgLi_2Ga$ phase and the β matrix. This mismatch is much larger than that of the Mg_3Al phase (−3.3%) [7]. It is not clear from the data collected whether the $MgLi_2Ga$ phase is the strengthening phase since the present techniques used are not adequate to detect nano sized precipitates. Therefore, it is necessary to perform a more in-depth analysis utilizing transmission electron microscopy or atom probe tomography to confirm the identification of the strengthening phase.

[0141] Solid solution strengthening in magnesium alloys is typically characterized utilizing the equation [18,19]:

$$\Delta\sigma_{SS} = kc^n \tag{3}$$

[0142] Where k is an elemental specific strengthening constant, c is the atomic fraction of solute, and n is a constant (½~⅔) [18]. Assuming the binary L12 alloy exhibits the same hardness to yield strength ratio as the Mg—Li—Ga alloys (σ_y=1.75HV), Ga solute has a k value of 770 and 1715 when n is ½ and ⅔, respectively. In comparison, the Mg—Li—Al system has k values of 681 and 1266 when n is ½ and ⅔, respectively [13]. Therefore, Ga exhibits more potent solid solution strengthening effects than Al.

Conclusions

[0143] The influence of Ga on the β-phase Mg—Li system was investigated. In this work, three alloys with 12 wt % Li and 2, 3, and 5 wt % Ga were cast and analyzed. It was found that:

[0144] The LG125 alloy possessed more Ga than what was soluble in the β-phase at 400° C., which resulted in residual secondary phases following homogenization while all secondary phases were dissolved in the LG122 and LG123 alloys.

[0145] Hardness trials revealed that the Mg—Li—Ga exhibits room temperature aging effects analogous to the Mg—Li—Al system.

[0146] As cast LG122 and LG123 exhibited brittle fracture while the LG125 alloy exhibited ductile fracture.

[0147] Upon homogenization, LG122 and LG123 exhibited ductile fracture while the LG125 alloy exhibited brittle fracture.

[0148] Significant precipitation strengthening occurred upon room temperature aging, but it resulted in brittle fracture within the alloys.

[0149] Ga exhibits more potent solid solution strengthening effects than Al in the β Mg—Li system.

REFERENCES FOR EXAMPLE 2

[0150] [1] W. Xu, N. Birbilis, G. Sha, Y. Wang, J. E. Daniels, Y. Xiao, M. Ferry, A high-specific-strength and corrosion-resistant magnesium alloy, Nature Materials. 14 (2015) 1229-1235. https://doi.org/10.1038/nmat4435.

[0151] [2] P. D. Frost, Magnesium-Lithium Alloys: A Review of Current Developments, Columbus, OH, 1962.

[0152] [3] S. Kamado, Y. Kojima, Deformability and strengthening of superlight Mg—Li alloys, Metallurgical Science and Tecnology. 16 (1998).

[0153] [4] X. Peng, W. C. Liu, G. H. Wu, Strengthening-toughening methods and mechanisms of Mg—Li alloy: a review, Rare Metals. 41 (2022) 1176-1188. https://doi.org/10.1007/s12598-021-01874-2.

[0154] [5] G. H. Park, J. T. Kim, H. J. Park, Y. S. Kim, H. J. Jeong, N. Lee, Y. Seo, J. Y. Suh, H. T. Son, W. M. Wang, J. M. Park, K. B. Kim, Development of lightweight Mg—Li—Al alloys with high specific strength, Journal of Alloys and Compounds. 680 (2016) 116-120. https://doi.org/10.1016/j.jallcom.2016.04.109.

[0155] [6] M. Chunjiang, D. Zhang, Q. Jining, H. Wenbin, S. Zhongliang, Aging behavior of Mg—Li—Al alloys, Trans. Nonferrous Met. Soc. China. 9 (1999) 772-777.

[0156] [7] S. Tang, T. Xin, W. Xu, D. Miskovic, G. Sha, Z. Quadir, S. Ringer, K. Nomoto, N. Birbilis, M. Ferry, Precipitation strengthening in an ultralight magnesium alloy, Nature Communications. (2019). https://doi.org/10.1038/s41467-019-08954-z.

[0157] [8] T. Xin, Y. Zhao, R. Mahjoub, J. Jiang, A. Yadav, K. Nomoto, R. Niu, S. Tang, F. Ji, Z. Quadir, D. Miskovic, J. Daniels, W. Xu, X. Liao, L.-Q. Chen, K. Hagihara, X. Li, S. Ringer, M. Ferry, Ultrahigh specific strength in a magnesium alloy strengthened by spinodal decomposition, Sci. Adv. 7 (2021). https://www.science.org.

[0158] [9] S. Zhang, R. Wu, F. Zhong, X. Ma, X. Wang, Q. Wu, Ultra-high strength Mg—Li alloy with B2 particles and spinodal decomposition zones, Fundamental Research. (2022). https://doi.org/10.1016/j.fmre.2022.01.023.

[0159] [10] V. H. Pauly, A. Weiss, H. Witte, Kubisch flachenzentrierte Legierungen der Zusammensetzung Li2MgX mit raumzentrierter Unterstruktur, Zeitschrift Fr Metallkunde. 59 (1969) 414.

[0160] [11] V. V. Kinzhibalo, E. V. Mel'nik, O. F. Zmiy, An Investigation of the Ternary Mg—Li (Ga, Ge, In, T I, Pb) Systems, Russian Metallurgy. (1979) 192-196.

[0161] [12] R. Hooper, Z. Bryan, M. v. Manuel, The Effect of Indium Additions on Mg—Li and Mg—Li—Al Alloys, J Radional Nucl Chem. (2013) 868-874. https://doi.org/10.1007/s10745-006-9094-1.

[0162] [13] G. H. Park, J. T. Kim, H. J. Park, Y. S. Kim, H. J. Jeong, N. Lee, Y. Seo, J. Y. Suh, H. T. Son, W. M. Wang, J. M. Park, K. B. Kim, Development of lightweight Mg—Li—Al alloys with high specific strength, Journal of Alloys and Compounds. 680 (2016) 116-120. https://doi.org/10.1016/j.jallcom.2016.04.109.

[0163] [14] B. H. Toby, R. B. von Dreele, GSAS-II: The genesis of a modern open-source all purpose crystallography software package, Journal of Applied Crystallography. 46 (2013) 544-549. https://doi.org/10.1107/S0021889813003531.

[0164] [15] ASTM E92-17, Standard Test Methods for Vickers Hardness and Knoop Hardness of Metallic Materials, 2017.

[0165] [16] D. A. Porter, K. E. Easterling, Phase Transformations in Metals and Alloys, Second, Chapman & Hall, 1992.

[0166] [17] D. J. Frankel, G. B. Olson, Design of Heusler Precipitation Strengthened NiTi— and PdTi-Base SMAs for Cyclic Performance, Shape Memory and Superelasticity. 1 (2015) 162-179. https://doi.org/10.1007/s40830-015-0017-0.

[0167] [18] C. H. Cáceres, D. M. Rovera, Solid solution strengthening in concentrated Mg—Al alloys, Journal of Light Metals. 1 (2001) 151-156. www.elsevier.com/locate/lightmetals.

[0168] [19] H. A. Roth, C. L. Davis, R. C. Thomson, Modeling solid solution strengthening in nickel alloys, Metallurgical and Materials Transactions A: Physical Metallurgy and Materials Science. 28 (1997) 1329-1335. https://doi.org/10.1007/s11661-997-0268-2.

Example 3

Experimental Procedures

[0169] Alloys were cast using a resistance furnace within a MBraun Labstar glovebox with a positive pressure argon (Ar) atmosphere (<50 ppm O2). Mg granules (99.8 wt pct Alfa Aesar), Li shot (99 wt pct Sigma Aldrich), and In shot (99.9 wt pct Alfa Aesar) were utilized for casting. Melting was performed at 750° C. in a stainless-steel crucible that was covered with a graphite lid. Pure metals were melted together for 20 minutes followed by three stirs with a graphite stir rod 5 minutes apart to ensure homogeneity. Following the third stir, the molten mixture was poured into a graphite mold. To provide lubrication and avoid contamination, the stainless-steel crucible, graphite stir rod, and graphite mold were coated in aerosol boron nitride.

[0170] Cast alloys were sent to MSE Supplies LLC for compositional analysis via inductively coupled plasma optical emission spectroscopy (ICP-OES). The measured values for each of the alloys are displayed in Table 5. Alloy compositions were selected to exhibit a BCC matrix and variable volume fraction of the $MgLi_2In$ phase according to the ternary phase diagram constructed by Kinzhibalo et al. at 300° C. [20]. The compositions denoted LI114, LI115, and LI1110 correspond to $MgLi_2In$ volume percent of 3, 5, and 10%, respectively.

TABLE 5

Alloy compositions measured via ICP-OES and nomenclature for alloys

Alloy	Mg at %	Li wt % (at %)	In wt % (at %)
LI114	Balance	11.2 (31.4)	4.1 (0.7)
LI115	Balance	11.3 (31.9)	5.3 (0.9)
LI1110	Balance	10.7 (31.5)	10.1 (1.8)

[0171] Homogenization heat treatments were performed on samples encapsulated in Pyrex tubes. Before inserting the samples into the tubes, all surface oxide was removed with 600 grit SiC paper followed by ultrasonic cleaning in isopropanol and wrapping the samples in 306 stainless steel foil to avoid contact with the tube. Encapsulation involved pulling a vacuum to ≤0.035 torr and backfilling to ~400 torr with ultra-high-purity Ar (99.999 wt %) before sealing. Homogenization was performed at 400° C. for 24 hours. Following homogenization, samples were quenched in water.

[0172] After homogenization, artificially aged alloys were sectioned into pieces roughly 1×1×3 mm with a low-speed saw and aged in an oil bath at 75° C. Samples were cooled to room temperature in air followed by mounting in epoxy. Hardness testing was performed using a Wilson Hardness tester with a load of 100 grams and hold time of 10 seconds. Five measurements were taken for each point and error bars were determined in accordance with ASTM E92 [21]. Room temperature aged samples were tested without mounting in epoxy.

[0173] Compression testing was performed using an Instron 3119 load frame. Cylindrical samples of height 17.5 mm and a 2-to-1 height-to-diameter ratio were utilized. A strain rate of 10-3 was used for each test. Three tests were performed for each condition and results were averaged. All tests for homogenized samples were performed within 10 minutes of quenching to minimize room temperature aging effects.

[0174] Scanning Electron Microscopy (SEM) images were acquired using a Tescan Mira3 microscope on samples mounted in epoxy with a maximum exotherm of ~65° C. and polished to a 0.05 μm finish. Grain size analysis was performed on these samples through etching with an acetal picric acid and utilizing imageJ to perform the linear intercept method. X-ray diffraction (XRD) was performed to identify phases present within the alloys using a Panalytical XPERT Powder machine. A Cu Kα x-ray beam was used with a step size of 0.008° and dwell time of 45 seconds per step. Powder samples were made by filing bulk samples followed by grinding with a mortar and pestle. Homogenized samples were tested within 30 minutes of quenching. Rietveld refinement was performed using the open source GSAS II code to obtain phase fractions and lattice parameters of the HCP, BCC, and $MgLi_2In$ phases.

Results

Microstructure

[0175] FIGS. **14***a*-**14***c* display the as-cast microstructure for the three Mg—Li—In alloys. It is observed that In rich secondary phases preferentially precipitated at the grain boundaries. XRD of these alloys in FIG. **13***a* reveals a BCC matrix with less than 15 volume percent HCP phase and variable $MgLi_2In$ phase. The inset in FIG. **13***a* displays significant peak broadening of the $MgLi_2In$ peaks which is indicative of either nano sized precipitates or a large number of lattice defects such as coherency strains or dislocations [23]. FIG. **14** contains a higher magnification micrograph of the as-cast LI114 alloy. It is observed that there are nano-scale round secondary phases that are strung within the matrix similar to the Mg—Li—Zn system [24]. A higher magnification image of the LI114 as-cast alloy reveals nano-scale precipitation in the matrix. The identification of these secondary phases is unknown since there are too small for accurate EDS measurements and they are not observed in the XRD pattern in FIG. **13***a*. However, their bright contrast in the BSE micrograph indicates their enrichment in In.

[0176] Homogenized micrographs of these alloys heat treated at 400° C. for 24 hr and quenched in water are displayed in FIGS. **17***a*-**17***c*. Upon homogenization, all of the In rich secondary phases dissolved out of the grain boundaries in the LI113 and LI115 alloys while there are some that still reside in the grain boundaries of the LI1110 alloy. Additionally, the nano-scale secondary phases displayed in FIG. **14** were also dissolved during the homogenization process. XRD in FIG. **13***b* displays that all alloys exhibit a BCC matrix with a small fraction of HCP phase. The LI115 and LI1110 alloys also exhibit a small degree of the $MgLi_2In$ phase following homogenization.

Aging Properties

[0177] The Mg—Li—In alloys exhibit aging characteristics at room temperature, similar to other Mg—Li based systems [10,14,25]. FIG. **16***a* displays the hardness measurements used to characterize room temperature aging within the Mg—Li—In alloys. It is observed that the initial hardness of the alloys increases upon greater In additions due in part to solid solution strengthening effects. This trend continues throughout the aging process with the higher In containing alloys exhibiting greater strength values. This is due to the higher supersaturation of In increasing the driving force for precipitate nucleation and growth resulting in greater overall strengths achieved [15]. Upon room temperature aging, the LI114, LI115, and LI1110 alloys exhibited hardness increases of 44, 53, and 49%, respectively, compared to the homogenized state. This indicates a significant degree of precipitation hardening upon room temperature aging. These alloys do not exhibit overaging following room temperature aging for 7,000Hr (292 days).

[0178] The effect of artificial aging on the Mg—Li—In alloys at 75° C. is displayed in FIG. **16***b*. It is important to note that these alloys were set in epoxy prior to testing. Therefore, there is roughly 12-24 hours of room temperature aging that occurred after artificial aging prior to hardness measurements. Typical age hardening characteristics are exhibited within these alloys which reach peak hardness within an hour; however, peak hardness is retained to longer hours. In contrast, the LA113 alloy overages within an hour at 80° C.[9].

Mechanical Properties

[0179] Results from compression testing of the Mg—Li—In alloys are displayed in FIG. **17**. Table 6 contains a summary of the yield strength (YS) results from these tests and corresponding grain sizes. It is once again observed that the alloy strength increases with increasing In content. The as-cast alloys in FIG. **17***a* exhibit significantly greater strength than the homogenized and aged samples in FIGS. **17***b* and **17***c*, respectively. However, these as-cast alloys exhibit very little strain hardening and brittle cracking likely due to the solutes in the grain boundaries. In contrast, the homogenized and RT aged alloys exhibit a greater resistance to cracking. Upon room temperature aging for 500Hr, the strength of the alloys increased 70, 51, and 21% from the homogenized state in the LI114, LI115, and LI1110 alloys, respectively.

[0180] A useful evaluation of a materials formability is through the assessment of the strain hardening exponent (n) from the Holloman equation [26]. This term can be calculated using the relationship [27]:

$$\sigma_t = K\epsilon_t^n \tag{1}$$

[0181] where σ_t is the true stress, $\in_t$ is the true strain, and K is a constant. The n values calculated for the different alloys and conditions are listed in Table 5. It is observed that the LI114 and LI115 exhibit comparable n values while the values for LI1110 are much lower for all conditions. Additionally, these values display that while the as-cast alloys exhibit superior strength values, they exhibit very low formability.

TABLE 5

Summary of compression results of MgLiIn alloys in the as cast, homogenized, and RT aged states and the corresponding calculated strain hardening exponent (n) and grain sizes.

Alloy	Condition	YS (MPa)	n	Grain Size (μm)
LI114	As-Cast	185 ± 5	0.068 ± 0.023	439 ± 172
	400° C. 24 Hr	84 ± 4	0.298 ± 0.016	545 ± 185
	RT 500 Hr	143 ± 5	0.161 ± 0.018	
LI115	As-Cast	214 ± 1	0.103 ± 0.029	289 ± 127
	400° C. 24 Hr	101 ± 1	0.280 ± 0.030	576 ± 167
	RT 500 Hr	153 ± 5	0.179 ± 0.009	
LI1110	As-Cast	243 ± 5	0.042 ± 0.002	295 ± 75
	400° C. 24 Hr	159 ± 5	0.187 ± 0.003	376 ± 97
	RT 500 Hr	192 ± 7	0.120 ± 0.020	

DISCUSSION

[0182] The Mg—Li—In alloys exhibit superior coarsening resistance compared to the Mg—Li—Al and other Mg—Li ternary systems [9, 10, 14]. Coarsening rates (k) follow the relationship [15]:

$$k \propto D\gamma \tag{2}$$

where D is the diffusion coefficient and γ is the interfacial energy. The diffusion coefficients have not been assessed for either the BCC Mg—Li—Al or Mg—Li—In systems and therefore cannot be compared at this time. A good indication of γ is the lattice mismatch (8) between the precipitate and matrix. Assuming the "cube on cube" alignment of the $MgLi_2In$ and BCC phases [10], the interphase mismatch is calculated using Eq. 3 [18].

$$\delta = \left(\frac{a_{MgLi_2In} - 2a_{BCC}}{2a_{BCC}}\right) \times 100 \tag{3}$$

where α is the lattice parameter of a given phase. Using the XRD pattern in FIG. **13**, the lattice parameters of the BCC matrix and $MgLi_2In$ phases were calculated to be 3.51 and 6.96 Å, respectively. Therefore, there is a relatively small lattice mismatch of 0.85%. This is likely a major cause for the significant resistance to overaging exhibited by the Mg—Li—In alloys in FIG. **16**. In contrast, the lattice mismatch of the metastable Mg_3Al phase within the Mg—Li—Al system is 3.3% [10]. This does not allow for significant precipitate growth before overaging [15]. Additionally, the Mg_3Al phase transforms to the stable AlLi phase upon coarsening which is incoherent and provides little strengthening effects compared to the coherent phase.

[0183] Assessment of the strain hardening exponent (n) provides information on the formability of a material since it is indicative of its ability to uniformly distribute deformation over a wide region [28]. This parameter is low in traditional HCP Mg alloys, such as AZ31 (n=0.10), due to the low accommodation for strain within the HCP system [29]. The high strength LA113 alloy exhibits a n value of 0.138 ten minutes after quenching [10]. Therefore, as is typical, the high strength LA113 alloy (~330 MPa 10 minutes after quenching) exhibits lower formability than the lower strength Mg—Li—In alloys after quenching.

Conclusions

[0184] Three Mg—Li—In alloys with 11 wt % Li and variable In content were cast and analyzed. It was found that these alloys exhibit room temperature aging kinetics similar to other Mg—Li based alloys. However, this system exhibited significant coarsening resistance compared to other ternary Mg—Li based alloys likely due to a lower lattice mismatch between the matrix and strengthening phase. Compression testing revealed that the as-cast alloys exhibit the greatest strength over homogenized and aged alloys. However, the as cast alloys exhibit brittle cracking upon deformation resulting in low workability.

REFERENCES FOR EXAMPLE 3

[0185] [1] H. Haferkamp, R. Boehm, U. Holzkamp, C. Jaschik, V. Kaese, M. Niemeyer, Alloy development, processing and applications in magnesium lithium alloys, Materials Transactions. 42 (2001) 1160-1166. https://doi.org/10.2320/matertrans.42.1160.

[0186] [2] H. Z. Ye, X. Y. Liu, Review of recent studies in magnesium matrix composites, Journal of Materials Science. 39 (2004) 6153-6171. https://doi.org/10.1023/B:JMSC. 0000043583.47148.31.

[0187] [3] H. Somekawa, T. Mukai, Effect of texture on fracture toughness in extruded AZ31 magnesium alloy, *Scripta* Materialia. 53 (2005) 541-545. https://doi.org/10.1016/j.scriptamat.2005.04.048.

[0188] [4] J. Wu, L. Jin, J. Dong, F. Wang, S. Dong, The texture and its optimization in magnesium alloy, Journal of Materials Science and Technology. 42 (2020) 175-189. https://doi.org/10.1016/j.jmst.2019.10.010.

[0189] [5] A. Tehranchi, B. Yin, W. A. Curtin, Solute strengthening of basal slip in Mg alloys, Acta Materialia. 151 (2018) 56-66. https://doi.org/10.1016/j.actamat.2018.02.056.

[0190] [6] S. Kamado, Y. Kojima, Deformability and strengthening of superlight Mg—Li alloys, Metallurgical Science and Tecnology. 16 (1998).

[0191] [7] P. D. Frost, Magnesium-Lithium Alloys: A Review of Current Developments, Columbus, OH, 1962.

[0192] [8] G. H. Park, J. T. Kim, H. J. Park, Y. S. Kim, H. J. Jeong, N. Lee, Y. Seo, J. Y. Suh, H. T. Son, W. M. Wang, J. M. Park, K. B. Kim, Development of lightweight Mg—Li—Al alloys with high specific strength, Journal of Alloys and Compounds. 680 (2016) 116-120. https://doi.org/10.1016/j.jallcom.2016.04.109.

[0193] [9] M. Chunjiang, D. Zhang, Q. Jining, H. Wenbin, S. Zhongliang, Aging behavior of Mg—Li—Al alloys, Trans. Nonferrous Met. Soc. China. 9 (1999) 772-777.

[0194] [10] S. Tang, T. Xin, W. Xu, D. Miskovic, G. Sha, Z. Quadir, S. Ringer, K. Nomoto, N. Birbilis, M. Ferry, Precipitation strengthening in an ultralight magnesium alloy, Nature Communications. 10 (2019). https://doi.org/10.1038/s41467-019-08954-z.

[0195] [11] C. Li, B. Deng, L. Dong, X. Liu, K. Du, B. Shi, Y. Dong, F. Peng, Z. Zhang, Effect of Zn addition on the microstructure and mechanical properties of as-cast BCC Mg-11Li based alloys, Journal of Alloys and Compounds. 895 (2022). https://doi.org/10.1016/j.jallcom.2021.162718.

[0196] [12] L. Qichi, C. Jianzhong, L. Hanwu, Quenching and Ageing Behaviors of Mg—Li—Zn Alloy, Trans. Nonferrous Met. Soc. China. 7 (1997) 40-44.

[0197] [13] A. Yamamoto, T. Ashida, Y. Kouta, K. B. Kim, S. Fukumoto, H. Tsubakino, Precipitation in Mg-(4-13)% Li-(4-5)% Zn Ternary Alloys, Science And Technology. 44 (2003) 619-624. https://doi.org/10.2320/matertrans.44.619.

[0198] [14] W. R. D. Jones, G. v. Hogg, The Stability of Mechanical Properties of Beta-Phase Magnesium-Lithium Alloys, Journal of the Institute of Metals. 85 (1956) 255-262.

[0199] [15] D. A. Porter, K. E. Easterling, Phase Transformations in Metals and Alloys, Second, Chapman & Hall, 1992.

[0200] [16] C. S. Jayanth, P. Nash, Factors affecting particle-coarsening kinetics and size distribution, Jornal of Materials Science. 24 (1989) 3041-3052.

[0201] [17] V. H. Pauly, A. Weiss, H. Witte, Kubisch flachenzentrierte Legierungen der Zusammensetzung Li2MgX mit raumzentrierter Unterstruktur, Zeitschrift Fr Metallkunde. 59 (1969) 414.

[0202] [18] D. J. Frankel, G. B. Olson, Design of Heusler Precipitation Strengthened NiTi— and PdTi-Base SMAs for Cyclic Performance, Shape Memory and Superelasticity. 1 (2015) 162-179. https://doi.org/10.1007/s40830-015-0017-0.

[0203] [19] R. Hooper, Z. Bryan, M. V. Manuel, The Effect of Indium Additions on Mg—Li and Mg—Li—Al Alloys, J Radional Nucl Chem. (2013) 868-874. https://doi.org/10.1007/s10745-006-9094-1.

[0204] [20] V. V. Kinzhibalo, E. V. Mel'nik, O. F. Zmiy, An Investigation of the Ternary Mg—Li (Ga, Ge, In, TI, Pb) Systems, Russian Metallurgy. (1979) 192-196.

[0205] [21] ASTM E92-17, Standard Test Methods for Vickers Hardness and Knoop Hardness of Metallic Materials, 2017.

[0206] [22] B. H. Toby, R. B. von Dreele, GSAS-II: The genesis of a modern open-source all purpose crystallography software package, Journal of Applied Crystallography. 46 (2013) 544-549. https://doi.org/10.1107/S0021889813003531.

[0207] [23] T. Ungár, Microstructural parameters from X-ray diffraction peak broadening, *Scripta* Materialia. 51 (2004) 777-781. https://doi.org/10.1016/j.scriptamat.2004.05.007.

[0208] [24] C. C. Hsu, J. Y. Wang, S. Lee, Room temperature aging characteristic of MgLiAlZn alloy, Materials Transactions. 49 (2008) 2728-2731. https://doi.org/10.2320/matertrans.MER2008225.

[0209] [25] H. J. Kleemola, M. A. Nieminen, On the Strain-Hardening Parameters of Metals, Metallurgical Transactions. 5 (1974) 1863-1866.

[0210] [26] J. H. Holloman, Mechanical Properties of Porosity-Free Beta Tricalcium Phosphate (β-TCP) Ceramic by Sharp and Spherical Indentations, Transactions of the Metallurgical Society of AIME. 162 (1945) 268-290. https://www.scirp.org/(S(351jmbntvnsjt1aadkposzje))/reference/ReferencesPapers.aspx?Refere nceID=699747 (accessed May 9, 2022).

[0211] [27] W. F. Hosford, Mechanical Behavior of Materials, Second Edition, Cambridge University Press, 2010.

[0212] [28] N. Afrin, D. L. Chen, X. Cao, M. Jahazi, Strain hardening behavior of a friction stir welded magnesium alloy, Scripta Materialia. 57 (2007) 1004-1007. https://doi.org/10.1016/j.scriptamat.2007.08.001.

[0213] It should be emphasized that the above-described embodiments of the present disclosure are merely possible examples of implementations set forth for a clear understanding of the principles of the disclosure. Many variations and modifications may be made to the above-described embodiment(s) without departing substantially from the spirit and principles of the disclosure. All such modifications and variations are intended to be included herein within the scope of this disclosure and protected by the following claims.

1. An alloy comprising

(a) gallium in the amount of from about 0.1 atomic percent to about 2 atomic percent or from about 0.5 weight percent to about 10 weight percent;

(b) lithium in the amount of from about 23 atomic percent to about 35 atomic percent or from about 8 weight percent to about 15 weight percent; and

(c) the balance of the alloy is magnesium.

2. The alloy of claim **1**, wherein gallium is in the amount of from about 0.1 atomic percent to about 2 atomic percent.

3. The alloy of claim **1**, wherein gallium is in the amount of from about 1 weight percent to about 5 weight percent.

4. The alloy of claim **1**, wherein lithium is in the amount of from about 23 atomic percent to about 31 atomic percent.

5. The alloy of claim **1**, wherein lithium is in the amount of from about 8 weight percent to about 12 weight percent.

6. The alloy of claim **1**, wherein gallium is in the amount of from about 0.1 atomic percent to about 1.5 atomic percent and lithium is in the amount of from about 23 atomic percent to about 31 atomic percent.

7. The alloy of claim **1**, wherein gallium is in the amount of from about 1 weight percent to about 5 weight percent and lithium is in the amount of from about 8 weight percent to about 12 weight percent.

8. An alloy comprising

(a) indium in the amount of from about 0.1 atomic percent to about 2 atomic percent or from about 2 weight percent to about 15 weight percent;

(b) lithium in the amount of from about 23 atomic percent to about 35 atomic percent or from about 10 weight percent to about 15 weight percent; and

(c) the balance of the alloy is magnesium.

9. The alloy of claim **8**, wherein indium is in the amount of from about 0.5 atomic percent to about 2 atomic percent.

10. The alloy of claim **8**, wherein indium is in the amount of from about 2 weight percent to about 10 weight percent.

11. The alloy of claim **8**, wherein lithium is in the amount of from about 23 atomic percent to about 31 atomic percent.

12. The alloy of claim **8**, wherein lithium is in the amount of from about 8 weight percent to about 12 weight percent.

13. The alloy of claim **8**, wherein indium is in the amount of from about 0.5 atomic percent to about 2 atomic percent and lithium is in the amount of from about 23 atomic percent to about 31 atomic percent.

14. The alloy of claim **8**, wherein indium is in the amount of from about 2 weight percent to about 10 weight percent and lithium is in the amount of from about 8 weight percent to about 12 weight percent.

15-21. (canceled)

22. The alloy of claim **1**, wherein the alloy has an X-ray powder diffraction pattern comprising $MgLi_2Ga$ face-centered cubic (FCC) based peaks at 23.3°, 27.0°, 38.5°, 45.5°, and 55.6°+0.2° 2θ as measured by X-ray powder diffraction using an x-ray wavelength of 1.54 Å.

23. The alloy of claim **8**, wherein the alloy has an X-ray powder diffraction pattern comprising $MgLi_2In$ face-centered cubic (FCC) based peaks at about 22.3°, 25.8°, 36.8°, and 43.5°+0.2° 2θ as measured by X-ray powder diffraction using an x-ray wavelength of 1.54 Å.

24. (canceled)

25. An alloy produced by the process comprising

(a) melting magnesium, lithium, and gallium or indium to produce a first composition;

(b) homogenizing the first composition to produce a predominately body-centered cubic (BCC) structure; and

(c) ageing the body-centered cubic (BCC) structure to produce the alloy.

26. (canceled)

27. (canceled)

28. (canceled)

29. An article comprising the alloy of claim **1**.

30. An article comprising the alloy of claim **8**.

31. An article comprising the alloy of claim **25**.

32. (canceled)

* * * * *